FOREWORD

The research work described in this report was performed by the Bell Aerosystems Company, Buffalo, New York for the Flight Dynamics Laboratory, Research and Technology Division, Wright Patterson Air Force Base, Ohio. The work was accomplished under Contract No. AF33(657)-7486, Project No. 8219, Task No. 821901 and entitled "Nonlinear Thermoelastic Effects on Hypersonic Stability and Control". Mr. H.M. Davis and J.E. Jenkins have been the Air Force Project Officers since the initiation of the program in November 1961. The study program was carried out by the Vehicle Structures Department of Bell Aerosystems Company under the technical direction of Mr. V. W. Donato until July 1962. Since then, Mr. J. R. Batt has been Technical Director.

Results of initial phases of the study program are presented in FDL-TDR-64-16, Parts I and II and FDL-TDR-64-42. This report presents results of additional nonlinear structural-aerodynamic interaction experiments and analyses conducted on a 45° delta wing.

The author wishes to express his appreciation to Messrs. E.J. Morris and F. Stefanik for their efforts in connection with the experimental phase of the study and to Mr. F. Braun for his general assistance throughout the entire program.

The digital computer FORTRAN program described in this report is available to eligible recipients from the Control Criteria Branch, Flight Control Division, A.F. Flight Dynamics Laboratory, Wright-Patterson A.F.B., Ohio, 45433.

This technical report has been reviewed and is approved.

C. R. Bryan
for W. A. Sloan, Jr.
Colonel USAF
Chief, Flight Control Division
AF Flight Dynamics Laboratory

ABSTRACT

Results are presented of additional nonlinear structural-aerodynamic interaction experiments and analyses conducted on a 45° delta wing. The aeroelastic simulation scheme developed and described in FDL-TDR-64-16 Part II was used to experimentally determine the static aerothermoelastic behavior of the subject model wing. Test data have been compared with theoretical predictions using the digital computer program developed and described in FDL-TDR-64-16, Part II.

CONTENTS

ILLUSTRATIONS

TABLES

SYMBOLS

c	wing chord
$\bar{c}$	wing average chord
q	dynamic pressure
X,Y,Z	rectangular coordinates
C_L	lift coefficient
E	modulus of elasticity
P_z	applied load
Q_o, Q_1, Q_2	aerodynamic influence coefficients
R	assigned reference point areas
α	equilibrium angle of attack
α_o	initial angle of attack due to P_{z_o}
α_g	geometric or rigid angle of attack
α_s	streamwise angles produced by elastic deformation
δ	displacement influence coefficient
$\frac{\Delta p}{q}$	nondimensional lifting pressure
Φ	loss of torsional stiffness parameter

SECTION 1.0
INTRODUCTION

The purpose of the study described herein and in References 1 to 3 is to determine, both experimentally and analytically, the combined influence of nonlinear aerodynamic and nonlinear structural behavior (through geometric large deflections and thermal effects) upon static aeroelastic interactions and attendant "flexible" stability and control derivatives. The overall objectives of the study were:

(1) To develop a technique for the simulation and measurement of static aeroelastic behavior in the presence of both aerodynamic and structural nonlinearities and elevated temperatures, as well as the actual measurement of data under such conditions.

(2) To formulate the governing mathematical relationships and development of a method and related computer program for the analysis of nonlinear static aeroelastic behavior.

(3) To conduct analyses and comparisons with test data obtained through objective (1).

(4) To develop a method for obtaining hypersonic aerodynamic influence coefficients.

(5) To conduct an exploratory examination of an experimental technique for measuring the slopes over the entire "field" of a deformed surface.

References 1, 2, and 3 describe previous experimental and analytical work associated with the above five objectives. Studies reported in Reference 1 showed that additional static aeroelastic interaction tests and analyses should be accomplished in order to further assess the present usefulness of the computer program developed under objective (2). Thus, a series of aeroelastic interaction tests and analyses were conducted on a 45° delta wing under both room and elevated temperature conditions. The simulation scheme developed under objective (1) was employed in these tests. The experimental program reported herein complements those tests previously conducted on an unswept wing model and introduces two important differences, namely;

Manuscript released by the author September 1964 for publication as an RTD Technical Documentary Report

swept wing structural behavior and associated analytical idealizations. The latter is of particular significance since the triangular plate elements and associated matrix relationships formulated under objective (2) can be evaluated.

The interaction tests described in this report provide additional experimental evidence of the importance of including nonlinear phenomena in static aeroelastic and stability and control analyses. The only other known efforts undertaken in this field are those tests and analyses reported in References 4 and 5. These research activities however, pertain only to linear aerodynamic-structural static interactions.

Section 2.0 of this report briefly discusses the simulation scheme developed in Reference 1 and its application to the subject test model. Test data are presented for a number of simulated dynamic pressures and angles of attack at room and at elevated temperatures. The analysis phase of the subject study is described in Section 3.0 and consisted of comparing selected test results with predicted test values. These were obtained from the digital computer program of Reference 1. Section 4.0 presents conclusions and recommendations.

SECTION 2.0

EXPERIMENTAL PROGRAM

2.1 SIMULATION TECHNIQUE

Figure 1 illustrates a representative lifting surface under test. Numerous reference points have been defined on the wing surface, but attention is directed toward instrumentation concentrated at a typical point, i. This same instrumentation would be located at all the reference points in an actual test setup. Figure 2 details the devices, instrumentation, and circuitry associated with the application of load and measurement of angular displacement at point i.

The static aeroelastic simulation technique described here pertains only to conditions where the aerodynamic load versus angular displacement relationship at each point is independent of such behavior elsewhere. The following expression is chosen as a representative applied load versus angular displacement relationship:

$$P_{z_i} = P_{z_{o_i}} + \bar{Q}_{1_i} \alpha_i + \bar{Q}_{2_i} \alpha_i^2 \qquad (1)$$

where

$$P_{z_{o_i}} = q R_i Q_{o_i}$$

$$\bar{Q}_{1_i} = q R_i Q_{1_i}$$

$$\bar{Q}_{2_i} = q R_i Q_{2_i}$$

R_i is the amount of surface area assigned to a reference point and Q_{o_i}, Q_{1_i}, Q_{2_i} are aerodynamic coefficients pertinent to the point in question. $P_{z_{oi}}$ is an initial load used to simulate angle of attack distributions at various dynamic pressure levels. (See Reference 1, pg 10).

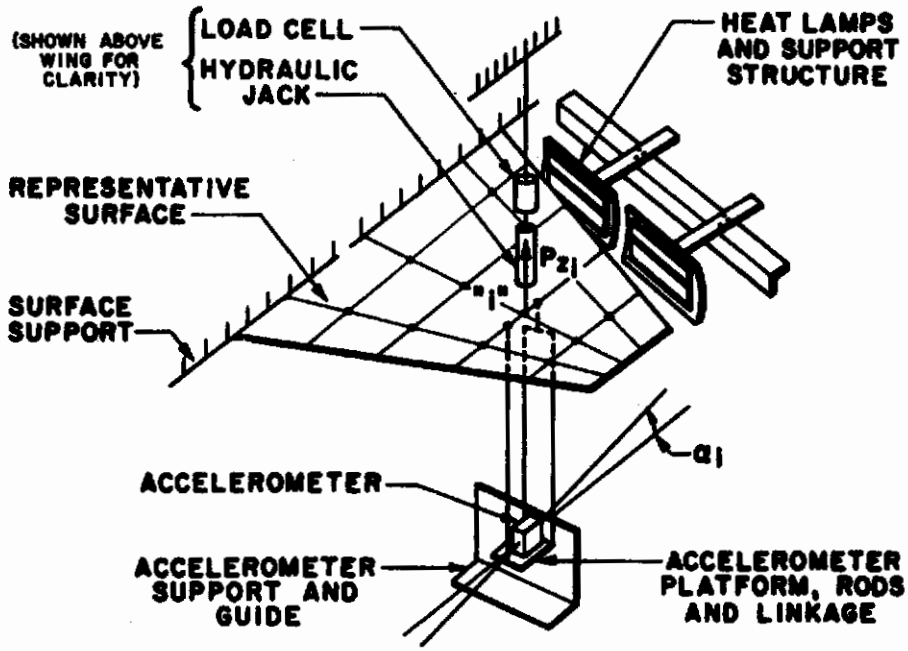

Figure 1. Lifting Surface Under Test

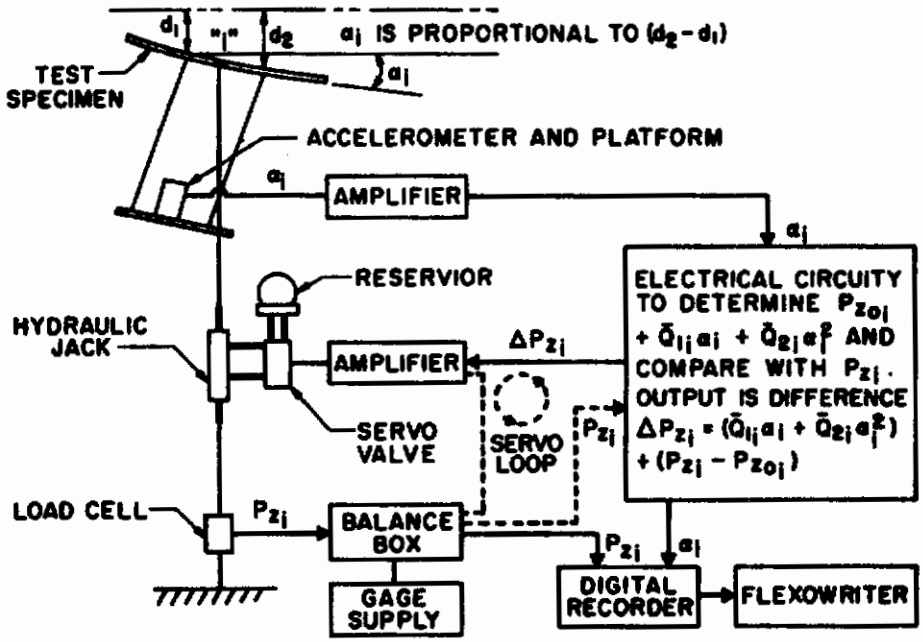

Figure 2. Aeroelastic Interaction Test Equipment and Instrumentation

Prior to test, the circuitry at each point (Figure 2) is provided with settings for $P_{z_{o_i}}$, $\bar{Q}_{1_i}$ and $\bar{Q}_{2_i}$. These settings are selected, using convenient analysis procedures, to represent aerodynamic conditions at a certain time in a flight profile. Since $P_{z_{o_i}}$ produces the effect of a geometric angle of attack the specimen may remain horizontal during test while angle-of-attack variations are introduced by proper adjustment of $P_{z_{o_i}}$.

An interaction test begins by imposing the system of initial loadings, $\{ P_{z_o} \}$, which immediately causes angular displacements, $\{ \alpha_o \}$, at all points. The magnitude of the initial angular displacement at point i, for example, is sensed by an accelerometer arrangement specially designed for this purpose and is transformed into a signal proportional to this magnitude. This signal, in turn, produces a signal for a new load P_{z_1} and compares this load with the initial load $P_{z_{o_i}}$. The resulting signal, proportional to ΔP_{z_i}, actuates a servo control valve and accordingly modifies the loading $P_{z_{o_i}}$. Thus, a first change in the load is produced as shown in Figure 2 and this change ΔP_{z_i} is, from Equation (1)

$$\Delta P_{z_i} = \bar{Q}_{1_i} \alpha_i + \bar{Q}_{2_i} \alpha_i^2 \qquad (2)$$

The load change, ΔP_{z_1}, causes additional angular displacements at the reference points. Hence, further adjustments of the load are obtained and the static aeroelastic process continues until the surface reaches an equilibrium position. A test cycle concludes with the measurement of equilibrium loads and slopes (i.e., angular displacements).

A basic instrumentation requirement for the above technique is a device which will accurately measure the chordwise angular displacement at a point on the surface of a wing in the presence of elevated temperatures. This requirement was met through the development of the arrangement shown in Figure 3 where the accelerometer is the critical element in the system which senses the direction of the gravity vector. The positioning of the accelerometer's sensitive axis in a horizontal plane produces a response in consequence of the acceleration due to gravity when the accelerometer undergoes an angular displacement. This measured acceleration

varies as the sine of the angle of displacement and has a maximum value of 1.0 (times g) when the sensitive axis is vertical. For the circumstances of interest, the angular displacements are quite small ($< 3^{\circ}$) and the accelerometer reading is proportional to the slope itself.

Since elevated temperature tests were to be conducted and the devices would not function properly in the resulting intense heat field, it was decided to mount each accelerometer at a distance from the wing surface. Figure 3 shows that the acceler-

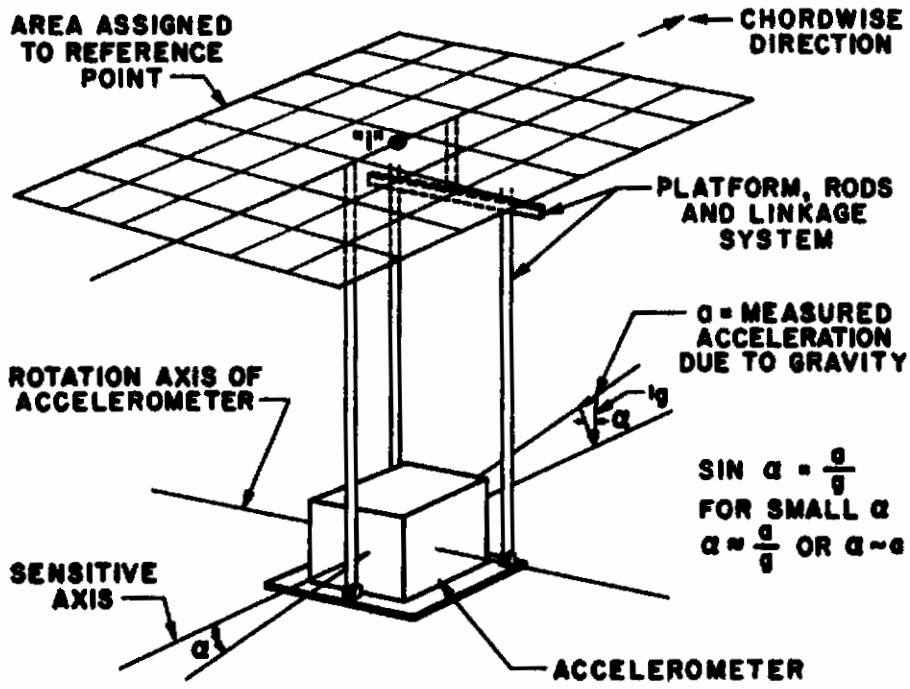

Figure 3. Angle Measuring Device

ometer is mounted on a 3-1/2 by 5 inch platform, which in turn is attached to the wing surface by means of three rods and a linkage system. The chordwise attachment to the wing surface occurs at two points that are 1-1/2 inches to either side of the associated reference point. The freedom of the platform to move was restricted to a vertical translation and rotation about a spanwise axis. From this arrangement, the accelerometer signal is proportional to $(d_2 - d_1)$, the difference in deflections at the two rod-wing specimen attachment points, rather than at the point i itself. Measurements taken for the purpose of establishing the accuracy of the above

scheme verified that it produces errors of less than 1 percent for angular displacements up to 5 degrees. Alternative schemes, involving the use of variable permeance extensometers were tried and found to yield slope measurements of insufficient accuracy. Furthermore, those on hand would "bottom-out" under displacements much smaller than those anticipated for actual testing.

The heating apparatus, load application system and data reduction equipment and techniques utilized were identical to those described in Reference 1 and hence are not discussed here. Figures 1 and 2 show their placement in the testing scheme.

2.2 TEST SPECIMEN

The specimen proportions, material properties, etc., were chosen as a compromise of a number of conflicting requirements, including the need to demonstrate low aspect ratio and large deflection effects while retaining a measure of simplicity for the sake of subsequent test-theory comparisons. Also, it was necessary that the large deflections neither exceed the "travel" limitations and capacity of available instrumentation nor introduce inelastic behavior. After reviewing these factors and the performance of preliminary static aeroelastic and stress analyses, it was decided that the model be of clipped delta planform with semispan of 32 inches, a root chord of 34 inches, and constant thickness of 0.528 inch. The specimen material is a steel alloy similar in composition to heat treated AISI type 4140 steel.

As shown in Figure 4, a total of 10 reference points is employed on the clipped delta semispan. All imposed loading and temperature conditions represented symmetric behavior of the wing as a whole, thus the same array of points was also delineated on the semispan not shown in Figure 4. The areas assigned to each reference point differ from point to point and are listed in Figure 10.

The specimen support assembly, pictured in Figure 5, consists of structural shapes which are welded together for rigidity. Screw jacks are used to maintain a clamping pressure on the 2 inch wide specimen support area. This arrangement was designed with the intent of minimizing root flexibility - i.e., to preclude vertical displacement or "roll" rotation of the wing root - while providing a small specimen contact area to minimize heat transfer from the model during elevated temperature tests.

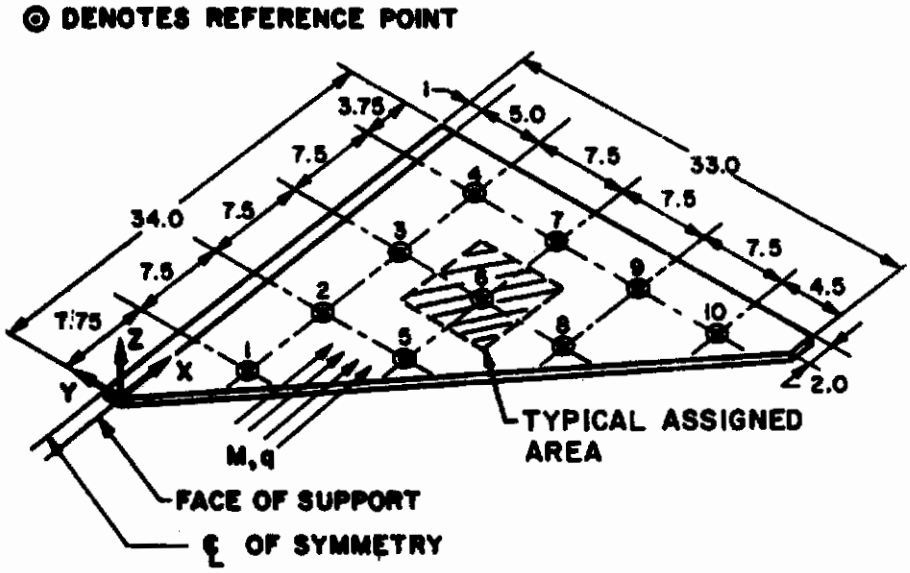

(All dimensions in inches)

Figure 4. Delta Wing Planform Specimen

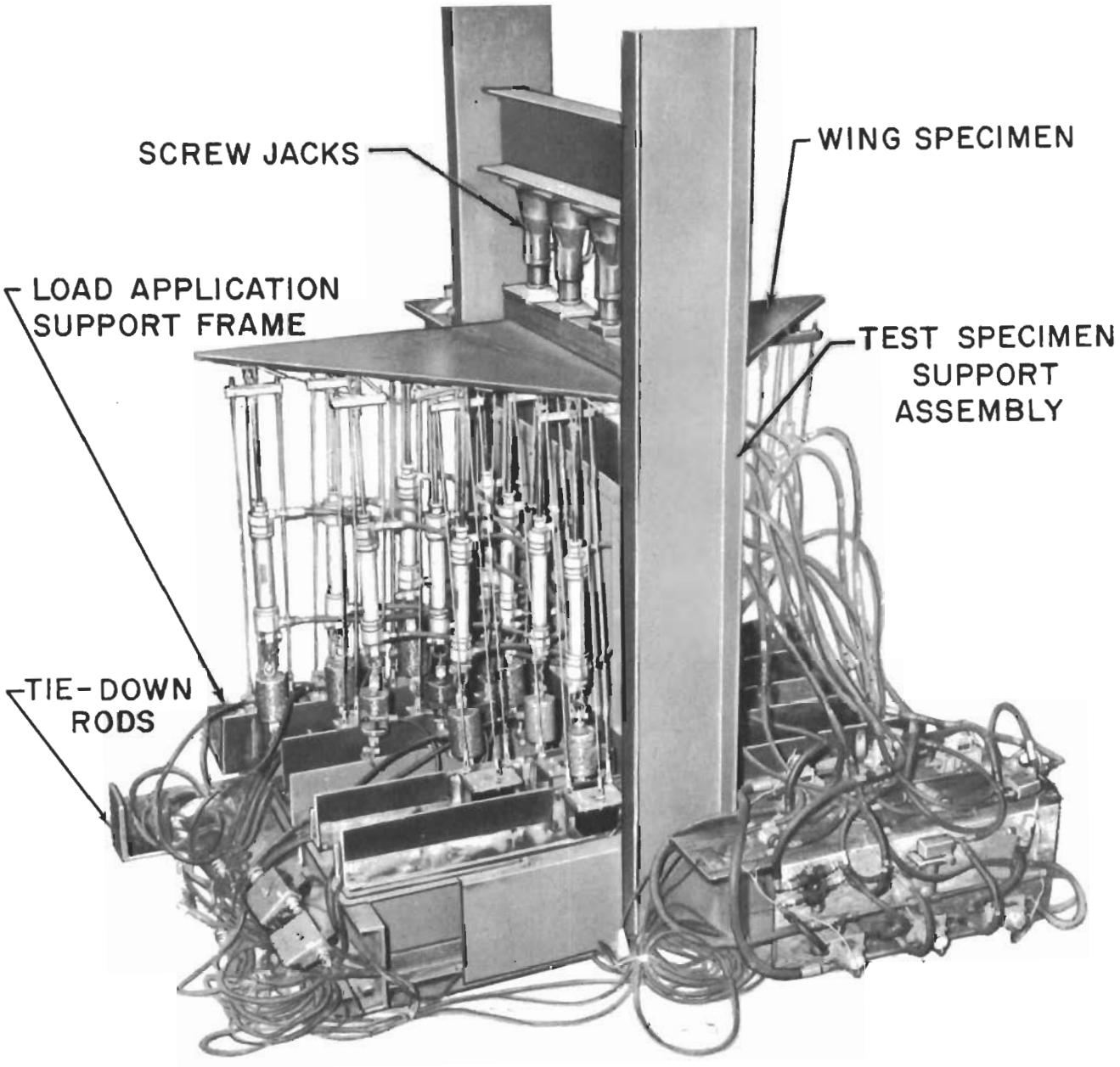

Figure 5. Test Specimen Support Structure

To provide accurate information for subsequent analytical studies, tests were performed to obtain the material mechanical properties and the coefficient of thermal expansion. Tests were performed at temperatures of 70, 350, 550, and 850°F., on coupons taken from the specimen sheet stock. Interpretation of the resulting data showed that the modulus of elasticity (E) can be satisfactorily represented as a function of temperature by the expression:

$$E = 30.79 \times 10^{6} - 1.099 \times 10^{4}\, T + 6.693\, T^{2}. \qquad (3)$$

Equation (3) is valid in the range of 70 to 800°F.

The average coefficient of thermal expansion was found to be essentially constant throughout this range of temperatures at a value of 7.0×10^{-6} in./in.°F. The material property tests were used to determine the yield stress and inelastic behavior characteristics of the parent material. This information was compared with the results of stress analyses to assess the possibility of inelastic deformation during test; it was predicted that no significant inelastic deformation would be sustained.

2.3 TEST RESULTS

Tests of the delta planform consist of:

(a) Interaction tests, at room temperature and also in the presence of elevated temperature for three dynamic pressures over the range of the three aerodynamic coefficients $\left\{P_{z_o}\right\}$ (pounds) $\left[\bar{Q}_1\right]$ (pounds/degree) and $\left[\bar{Q}_2\right]$ (pounds/degrees)^2) listed in Tables 1 to 3. Note that an abbreviated notation is used in these tables. For example, at room temperature test conditions, Table 1, q = 6 psi, only the diagonal elements of $\left[\bar{Q}_1\right]$ and $\left[\bar{Q}_2\right]$ are listed. $\left\{P_{z_o}\right\}$ is an initial loading column and $\left\{\alpha_o\right\}$ is the resultant initial angle of attack distribution. The equilibrium angles of attack (in degrees) and loads (in pounds) are denoted by $\left\{\alpha\right\}$ and $\left\{P_z\right\}$ respectively. (The results of these tests are described below.)

(b) Tests at room temperature for deflection and slope influence coefficients. (For convenience these coefficients are presented and discussed in Section 3.3.1 and Figures 11 and 12.)

As indicated in the discussion of the analytical basis of the static aerothermoelastic problem (see Reference 1) a reference point angle of attack (α_i) is a function

TABLE 1

DELTA PLANFORM AERODYNAMIC COEFFICIENTS AND TEST RESULTS; q = 6 psi

Test	Ref. Pts.	$[\bar{Q}_1]$	$[\bar{Q}_2]$	Load Condition No. 1				Load Condition No. 2				Load Condition No. 3				Load Condition No. 4			
				$\{P_{z_0}\}$	$\{\alpha_0\}$	$\{P_z\}$	$\{\alpha\}$	$\{P_{z_0}\}$	$\{\alpha_0\}$	$\{P_z\}$	$\{\alpha\}$	$\{P_{z_0}\}$	$\{\alpha_0\}$	$\{P_z\}$	$\{\alpha\}$	$\{P_{z_0}\}$	$\{\alpha_0\}$	$\{P_z\}$	$\{\alpha\}$
Room Temperature	1	-326	57	121	-0.0230	136	-0.0350	215	-0.0500	239	-0.0700	317	-0.0753	353	-0.1104	405	-0.1079	459	-0.1562
	2	-241	60	0	-0.0176	5	-0.0202	0	-0.0277	10	-0.0428	0	-0.0452	10	-0.0703	0	-0.0554	13	-0.0630
	3	-206	42	0	-0.0050	1	-0.0050	0	-0.0151	5	-0.0226	0	-0.0176	8	-0.0403	0	-0.0301	11	-0.0552
	4	+172	24	0	+0.0076	2	+0.0101	0	+0.0126	2	+0.0101	0	+0.0075	1	+0.0100	0	+0.0075	1	+0.0125
	5	-383	18	126	-0.0653	162	-0.0979	218	-0.1305	284	-0.1807	318	-0.1908	426	-0.2836	402	-0.2545	546	-0.3755
	6	-295	36	0	-0.0328	14	-0.0479	0	-0.0605	22	-0.0882	0	-0.0958	41	-0.1411	0	-0.1305	56	-0.1983
	7	-295	36	0	-0.0025	2	-0.0075	0	-0.0050	4	-0.0151	0	-0.0176	12	-0.0452	0	-0.0252	14	-0.0529
	8	-383	18	120	-0.0728	154	-0.1029	208	-0.1355	280	-0.1908	312	-0.2033	430	-0.3012	404	-0.0276	557	-0.4041
	9	-295	36	0	-0.0328	14	-0.0479	0	-0.0630	25	-0.0907	0	-0.1054	51	-0.1606	0	-0.1260	55	-0.2016
	10	-397	32	118	-0.0525	149	-0.0825	214	-0.1050	266	-0.1475	310	-0.1619	411	-0.2454	409	-0.2167	537	-0.3251
	C_{L_F}/C_{L_R}			1.318				1.330				1.386				1.388			
Thermal Test	1	-326	57	119	-0.0288	135	-0.0493	217	-0.0601	246	-0.0934	316	-0.1001	360	-0.1551	404	-0.1414	473	-0.2152
	2	-241	60	0	-0.0125	6	-0.0249	0	-0.0299	13	-0.0456	0	-0.0510	22	-0.0872	0	-0.0598	22	-0.0997
	3	-206	42	0	-0.0075	2	-0.0117	0	-0.0137	7	-0.0282	0	-0.0262	10	-0.0406	0	-0.0349	13	-0.0573
	4	+172	24	0	+0.0125	2	+0.0125	0	+0.0100	4	+0.0168	0	+0.0188	4	+0.0208	0	+0.0138	2	+0.0138
	5	-383	18	116	-0.0800	165	-0.1199	215	-0.1453	304	-0.2191	317	-0.2111	450	-0.3269	412	-0.2779	585	-0.4356
	6	-295	36	0	-0.0422	22	-0.0702	0	-0.0732	23	-0.0752	0	-0.1156	57	-0.1856	0	-0.1528	77	-0.2510
	7	-295	36	0	-0.0025	4	-0.0125	0	-0.0075	5	-0.0175	0	-0.0199	11	-0.0466	0	-0.0274	23	-0.0648
	8	-383	18	124	-0.0816	171	-0.1328	219	-0.1620	319	-0.2498	311	-0.2472	449	-0.3619	409	-0.3031	591	-0.4769
	9	-295	36	0	-0.0298	10	-0.0429	0	-0.0694	31	-0.1049	0	-0.1058	40	-0.1680	0	-0.1347	68	-0.2305
	10	-397	32	120	-0.0679	163	-0.1031	218	-0.1283	295	-0.1962	321	-0.1918	427	-0.2840	415	-0.2407	573	-0.3885
	C_{L_F}/C_{L_R}			1.419				1.434				1.447				1.484			

TABLE 2

DELTA PLANFORM – AERODYNAMIC COEFFICIENTS AND TEST RESULTS, q = 8 psi

Test	Ref. Pts.	$\bar{Q}_1$	$\bar{Q}_2$	Load Condition No. 1				Load Condition No. 2				Load Condition No. 3				Load Condition No. 4			
				$\{P_{z_o}\}$	$\{\alpha_o\}$	$\{P_z\}$	$\{\alpha\}$	$\{P_{z_o}\}$	$\{\alpha_o\}$	$\{P_z\}$	$\{\alpha\}$	$\{P_{z_o}\}$	$\{\alpha_o\}$	$\{P_z\}$	$\{\alpha\}$	$\{P_{z_o}\}$	$\{\alpha_o\}$	$\{P_z\}$	$\{\alpha\}$
Room Temperature	1	-435	76	157	-0.0351	183	-0.0602	283	-0.0731	337	-0.1235	416	-0.1054	496	-0.1857	643	-0.1726	787	-0.3110
	2	-321	80	0	-0.0200	12	-0.0375	0	-0.0402	20	-0.0728	0	-0.0602	33	-0.1130	0	-0.0922	56	-0.1818
	3	-275	56	0	-0.0176	6	-0.0227	0	-0.0201	14	-0.0477	0	-0.0301	17	-0.0628	0	-0.0428	32	-0.0984
	4	+229	32	0	+0.0101	3	+0.0126	0	+0.0151	3	+0.0201	0	+0.0176	3	+0.0151	0	+0.0076	4	+0.0145
	5	-510	24	156	-0.0950	232	-0.1550	282	-0.1732	435	-0.3037	414	-0.2575	645	-0.4550	645	-0.4048	1037	-0.7426
	6	-393	48	0	-0.0450	27	-0.0800	0	-0.0904	59	-0.1581	0	-0.1300	92	-0.2400	0	-0.2061	166	-0.4058
	7	-393	48	0	-0.0050	3	-0.0126	0	-0.0101	16	-0.0304	0	-0.0252	25	-0.0680	0	-0.0340	46	-0.1259
	8	-510	24	158	-0.1004	238	-0.1606	286	-0.1843	450	-0.3137	416	-0.2743	660	-0.4826	639	-0.4293	1077	-0.8237
	9	-393	48	0	-0.0428	26	-0.0731	0	-0.0832	59	-0.1512	0	-0.1260	95	-0.2394	0	-0.1991	174	-0.4245
	10	-529	43	156	-0.0680	214	-0.1210	279	-0.1406	408	-0.2435	407	-0.2108	608	-0.3790	649	-0.3478	1010	-0.6807
	C_{L_F}/C_{L_R}			1.501				1.594				1.618				1.704			
Thermal Test	1	-435	76	159	-0.0462	196	-0.0887	286	-0.0817	356	-0.1584	415	-0.1273	535	-0.2540	645	-0.2406	848	-0.4328
	2	-321	80	0	-0.0200	11	-0.0374	0	-0.0277	27	-0.0821	0	-0.0540	41	-0.1266	0	-0.0996	75	-0.2165
	3	-275	56	0	-0.0113	10	-0.0338	0	-0.0364	17	-0.0564	0	-0.0345	27	-0.0859	0	-0.0602	46	-0.1492
	4	+229	32	0	+0.0075	1	+0.0062	0	+0.0114	4	+0.0170	0	+0.0088	-	-	0	+0.0124	7	+0.0310
	5	-510	24	157	-0.1133	277	-0.2265	288	-0.1907	497	-0.3691	419	-0.2783	734	-0.5639	640	-0.4398	1163	-0.9723
	6	-393	48	0	-0.0510	41	-0.1119	0	-0.0876	73	-0.1828	0	-0.1370	125	-0.3151	0	-0.2188	241	-0.5638
	7	-393	48	0	-0.0150	6	-0.0376	0	-0.0175	21	-0.0639	0	-0.0375	47	-0.1275	0	-0.0611	101	-0.2530
	8	-510	24	162	-0.1241	294	-0.2520	284	-0.2083	497	-0.4127	410	-0.3079	741	-0.6417	644	-0.4733	1246	-1.0982
	9	-393	48	0	-0.0567	49	-0.1273	0	-0.0960	78	-0.1995	0	-0.1450	135	-0.3425	0	-0.2213	271	-0.6225
	10	-529	43	167	-0.1007	280	-0.2001	288	-0.1703	466	-0.3268	425	-0.2497	718	-0.5422	640	-0.3914	1241	-1.0246
	C_{L_F}/C_{L_R}			1.791				1.777				1.859				2.040			

TABLE 3

DELTA PLANFORM - AERODYNAMIC COEFFICIENTS AND TEST RESULTS, q = 10 psi

Test	Ref. Pts.	$[\bar{Q}_1]$	$[\bar{Q}_2]$	Load Condition No. 1				Load Condition No. 2				Load Condition No. 3				Load Condition No. 4			
				$\{P_{z_o}\}$	$\{\alpha_o\}$	$\{P_z\}$	$\{\alpha\}$	$\{P_{z_o}\}$	$\{\alpha_o\}$	$\{P_z\}$	$\{\alpha\}$	$\{P_{z_o}\}$	$\{\alpha_o\}$	$\{P_z\}$	$\{\alpha\}$	$\{P_{z_o}\}$	$\{\alpha_o\}$	$\{P_z\}$	$\{\alpha\}$
Room Temperature	1	-544	95	200	-0.0500	263	-0.1138	362	-0.0925	490	-0.2275	516	-0.1400	739	-0.3825	679	This test condition		
	2	-418	100	0	-0.0286	29	-0.0685	0	-0.0523	66	-0.1520	0	-0.0820	107	-0.2360	0	attempted but not		
	3	-343	70	0	-0.0113	9	-0.0263	0	-0.0299	45	-0.0922	0	-0.0453	72	-0.1433	0	recorded since		
	4	+286	40	0	+0.0075	2	+0.0088	0	+0.0100	1	+0.0025	0	+0.0125	8	+0.0275	0	a) Accelerometer		
	5	-638	30	199	-0.1255	381	-0.2811	361	-0.2175	727	-0.5625	521	-0.3267	1148	-0.9185	679	platform #10		
	6	-491	60	0	-0.0650	77	-0.1538	0	-0.1167	169	-0.3326	0	-0.1658	293	-0.5542	0	"bottomed-out"		
	7	-491	34	0	-0.0075	17	-0.0351	0	-0.0201	55	-0.1132	0	-0.0351	124	-0.2507	0	b) System did not		
	8	-638	30	199	-0.1316	388	-0.2935	357	-0.2400	757	-0.6275	520	-0.3562	1226	-1.0811	678	reach equilib-		
	9	-491	60	0	-0.0588	73	-0.1475	0	-0.1082	158	-0.3171	0	-0.1712	329	-0.6267	0	rium state.		
	10	-661	54	200	-0.1041	356	-0.2359	355	-0.1926	723	-0.5170	524	-0.2873	1224	-0.9500	673			
	C_{L_F}/C_{L_R}			2.00				2.224				2.532				—			
Thermal Test	1	-544	95	199	-0.0206	286	-0.1560	355	-0.1097	547	-0.3174	519	-0.1538	809	-0.4799	680	This test condition		
	2	-418	100	0	-0.0250	36	-0.0913	0	-0.0485	70	-0.1691	0	-0.0746	111	-0.2486	0	attempted but not		
	3	-343	70	0	-0.0167	40	-0.0499	0	-0.0326	58	-0.1230	0	-0.0465	81	-0.1707	0	recorded since		
	4	+286	40	0	+0.0143	5	+0.0188	0	+0.0099	4	+0.0132	0	+0.0037	13	+0.0448	0	a) Accelerometer		
	5	-638	30	202	-0.1414	461	-0.3797	360	-0.2324	835	-0.7040	519	-0.3418	1226	-1.056	679	platform #10		
	6	-491	60	0	-0.0755	117	-0.2279	0	-0.1207	230	-0.4248	0	-0.1829	345	-0.6543	0	"bottomed-out"		
	7	-491	34	0	-0.0075	35	-0.0639	0	-0.0225	84	-0.1705	0	-0.0424	161	-0.3083	0	b) System did not		
	8	-638	30	203	-0.1502	467	-0.4085	356	-0.2568	877	-0.8010	516	-0.3802	1361	-1.264	680	reach equilib-		
	9	-491	60	0	-0.0619	91	-0.1967	0	-0.1147	209	-0.4332	0	-0.1610	386	-0.7220	0	rium state.		
	10	-661	54	206	-0.1170	441	-0.3215	355	-0.2090	852	-0.6483	512	-0.3091	1429	-1.239	681			
	C_{L_F}/C_{L_R}			2.443				2.641				2.870				—			

of the aerodynamic parameters q and α_g, the deformational characteristics of the structure, and the temperature environment. Since it was intended to isolate, insofar as possible, the relative significance of the respective aerodynamic parameters and the temperature effects, a large number of tests on the delta planform specimen was performed. .

Variations of the aerodynamic parameters q and α_g are accomplished through variation of the aerodynamic coefficients $\left\{P_{z_o}\right\}$, $\left[\bar{Q}_1\right]$, $\left[\bar{Q}_2\right]$. Equation (1), written in matrix form, shows that

$$\begin{aligned} \left\{P_{z_o}\right\} &= q \left[R\right] \left[Q_o\right] \left\{1\right\} \\ \left[\bar{Q}_1\right] &= q \left[R\right] \left[Q_1\right] \\ \left[\bar{Q}_2\right] &= q \left[R\right] \left[Q_2\right] \end{aligned} \qquad (4)$$

Different values of q can be simulated by simply ratioing the values of the aerodynamic coefficients to certain initial values. As previously described the "effective" angle of attack is varied by simply changing the initial loads $\left\{P_{z_o}\right\}$. Initial loads were imposed on the test specimen at reference points 1, 5, 8, and 10. The aerodynamic coefficients listed in Tables 1 to 3 were obtained by ratioing an initial set of aerodynamic coefficients as determined by preliminary static aeroelastic analyses performed for specimen design purposes.

Eleven room temperature tests were conducted followed by eleven elevated temperature tests. Each set of data in Tables 1 to 3 represents the selection of test points obtained from two or more test runs. It was found necessary to increase the number of runs at elevated temperatures in order to achieve an acceptable degree of data repeatability. Study of all data recorded showed that the repeatability of the simulation scheme is within 3% at room temperature and 11% at elevated temperatures. The percentage increase at elevated temperatures was due to increased difficulty in maintaining initial accelerometer zero levels and servovalve settings.

The desired temperature distributions were to possess a significant nonlinear variation in both chord and span directions with maximum temperatures occurring along the leading edge. Figure 6 illustrates the temperature profile obtained (temperature values at the planform reference points are tabulated in Figure 10). This profile was continually reproduced within 10-15°F for each of the test conditions cited in Tables 1 to 3. Thermocouples affixed to the test specimen indicated that there were small temperature differences (< 6°F) across the specimen thickness and only a small drop in temperature (< 20°F) through the root support.

Variation of the measured equilibrium angles of attack at the leading edge reference points is shown in Figure 7 for both room and elevated temperatures and represent typical results. Study of Figures 7a and 7b will show that large increases in the equilibrium angle of attack were obtained as q was increased. The change in these angles due to elevated temperature is displayed in Figure 7c; it is evident that significant percentage increases were obtained. It is to be noted here that thermal effects have been introduced in the manner shown in Figure 7 since the loss in torsional stiffness parameter, Φ , as used in Reference 1 cannot be realistically defined for the subject test specimen.

Figure 8 displays the variation of the equilibrium angle of attack at reference point ten, α_{10}, as a function of load condition and dynamic pressure. The dashed lines in this figure represent a probable extrapolation path to q = 10 psi, load condition No. 4 test point. Data at this test condition was not obtained since the accelerometer platform at reference point ten "bottomed-out" resulting in a nonequilibrium state. Recalling that sets of initial loads are utilized to simulate an initial angle of attack distribution, it is seen from Figures 8a and 8b that this parameter has an important effect on the equilibrium angle of attack. However, larger increases in α_{10} are obtained by varying the dynamic pressure levels. The effect of temperature upon α_{10} is shown in Figure 8c and is seen to be substantial at the higher load conditions and dynamic pressure levels.

Additional test results are shown in Figure 9 by displaying the ratio of flexible to rigid lift coefficients as a function of load condition, dynamic pressure and

temperature environment. This ratio was derived from the equilibrium loads by summing the loading columns at each load condition. Study of these data shows that the rate of change of C_{L_F}/C_{L_R} with initial load (initial angle of attack) increases as the dynamic pressure is increased. The effect of temperature, of course, is seen to increase the subject ratio above the room temperature value. The dashed lines indicate, as in the previous figure, data extrapolation.

It is concluded from the tests conducted that the interplay between aerodynamic and structural nonlinearities (through geometric large deflections and thermal effects) is significant and of importance in determining the static aeroelastic behavior of a lifting surface. The series of tests conducted also provides additional evidence that the technique for simulation of nonlinear static aerothermoelastic behavior is a feasible and successful one within the limitations of the original assumption regarding the exclusive dependence of additional aerodynamic load on local angle of attack.

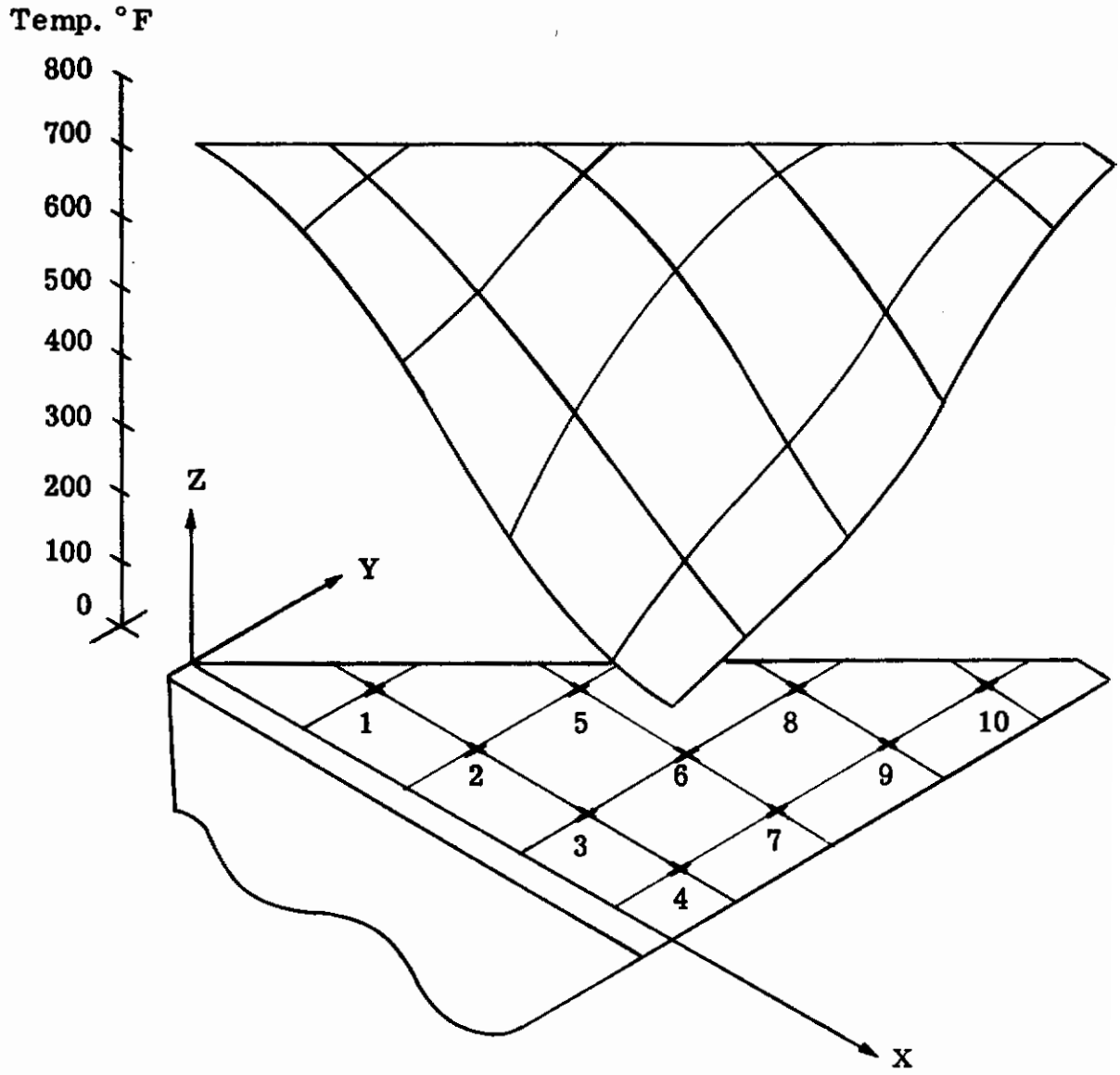

Figure 6. Delta Planform Temperature Distribution

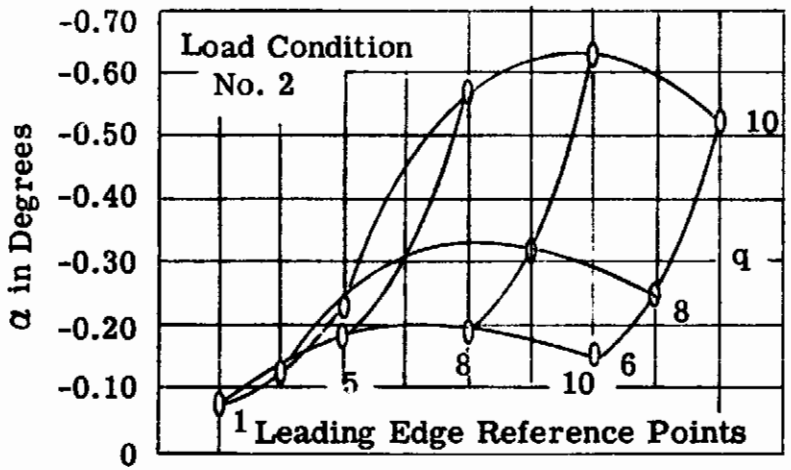

Figure 7a. Room Temperature

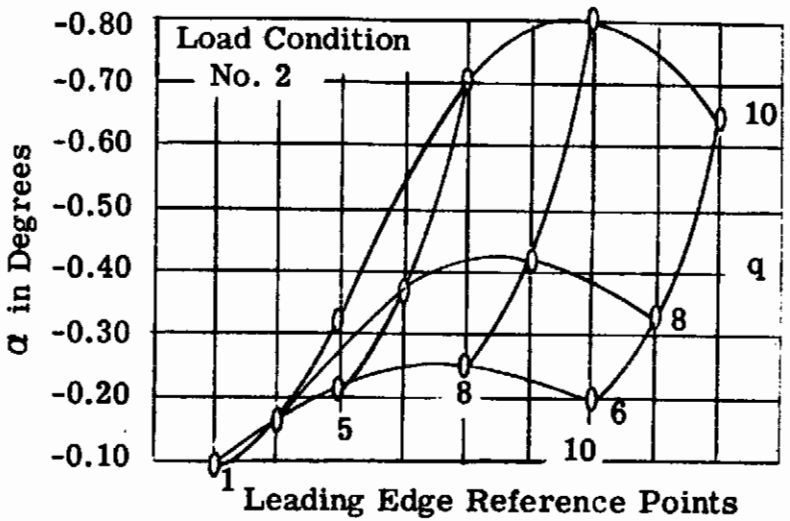

Figure 7b. Elevated Temperature

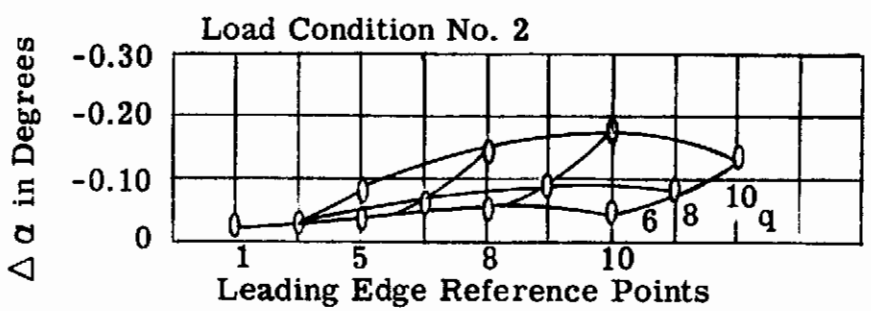

Figure 7c. Change In α Due To Elevated Temperature

Figure 7. Selected Test Results - Equilibrium Angles of Attack

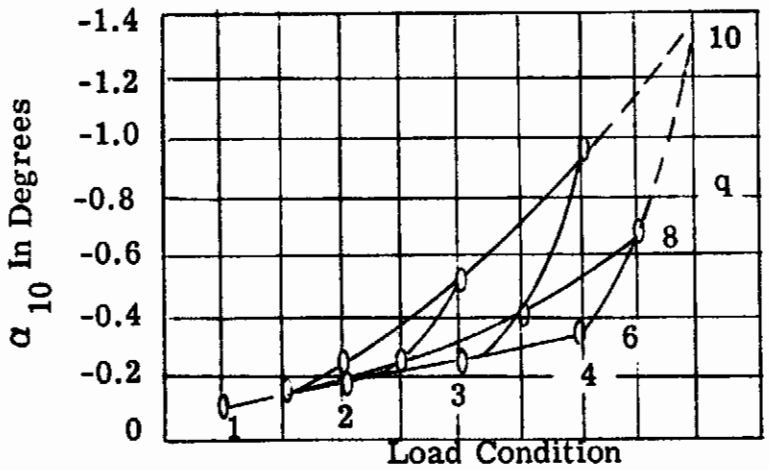

Figure 8a. Room Temperature

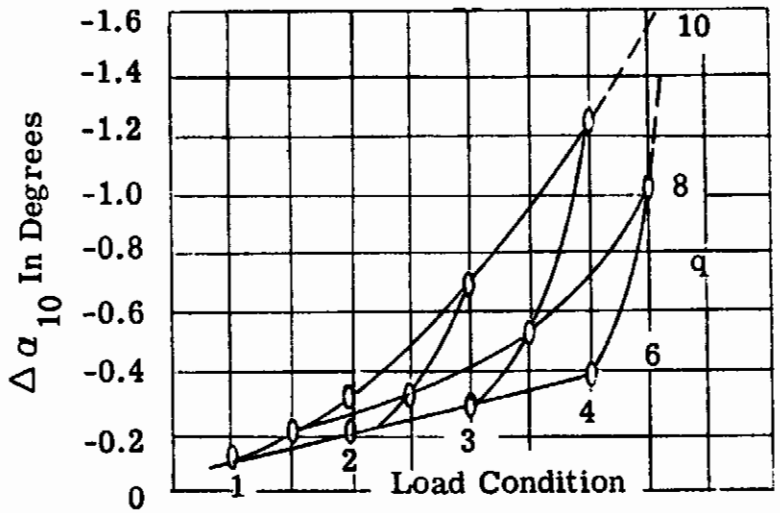

Figure 8b. Elevated Temperature

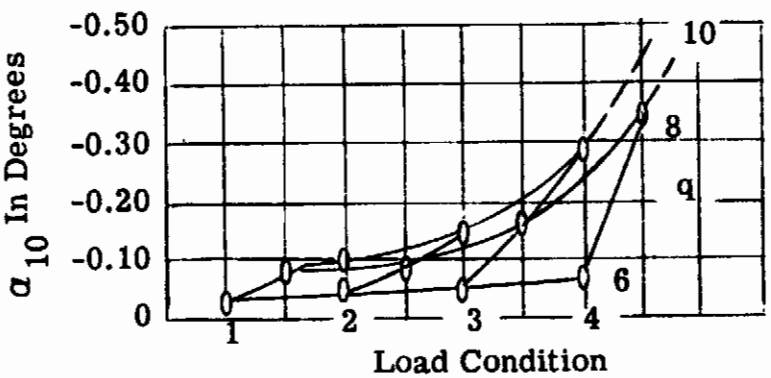

Figure 8c. Change In α_{10} Due To Elevated Temperature

Figure 8. Selected Test Results - Equilibrium Angle of Attack, α_{10}

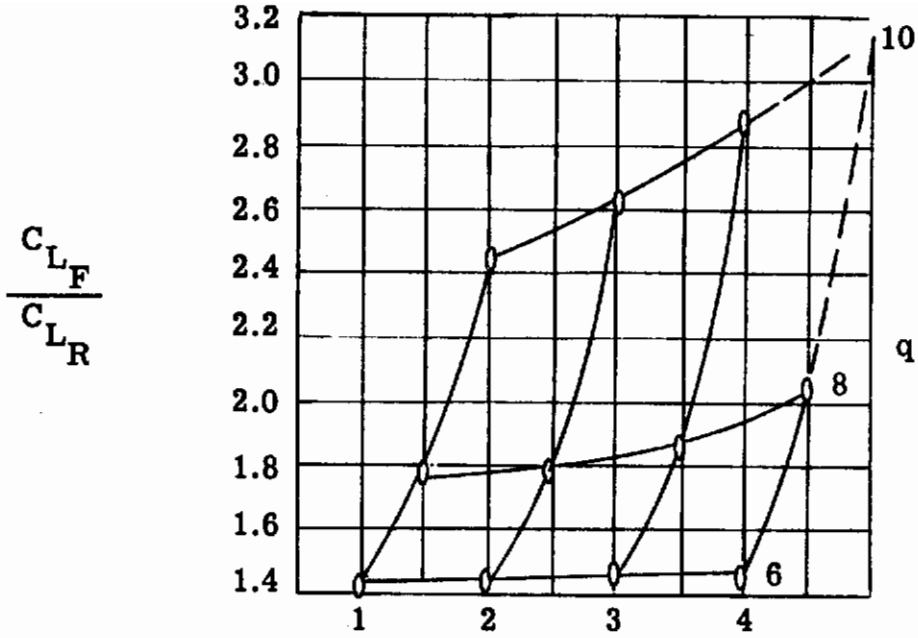

Figure 9b. Elevated Temperature

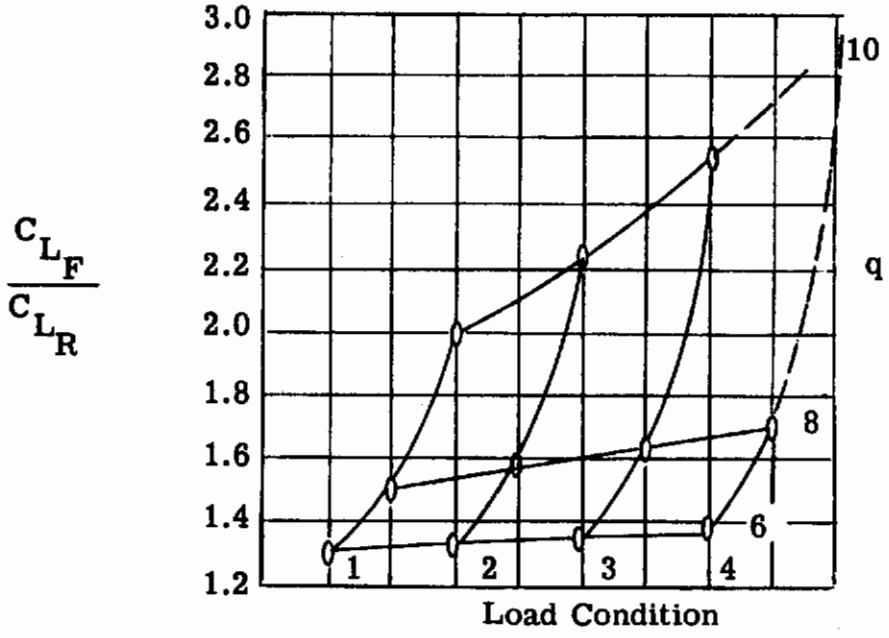

Figure 9a. Room Temperature

Figure 9. Selected Test Results - Ratio Of Flexible To Rigid Lift Coefficient

SECTION 3.0
THEORY-TEST COMPARISONS

3.1 GENERAL

The objectives of the subject study contract, as described in Reference 1, included the development of an analytical method and related computer program for the analysis of nonlinear static aeroelastic behavior and comparisons of the results of such analyses with selected test data of the previous section. Analyses were conducted at room and elevated temperatures for several values of the dynamic pressure. Both linear and nonlinear structural behavior in combination with nonlinear aerodynamic behavior was considered.

3.2 INPUT DATA

Input to the computer program consists of structural and aerodynamic analysis data, respectively. Two major options are available in connection with the structural analysis portion of the program: (1) the basic material property, geometric and temperature data is given so that the computer automatically develops the set of structural influence coefficients; or (2) the structural influence coefficients are provided as input. In the case of option (1), the input specifically consists of the coordinates of the reference points, the type and location of the discrete elements of the structural idealization, material properties, temperatures, boundary conditions, and initial displacements. The structural analysis input also includes a specification of a convergence criterion and the number of iterations allowed for convergence before the program will stop.

Aerodynamic input consists of sets of matrices defining aerodynamic influence coefficients, angle of attack distributions, assigned reference point areas, wing geometric properties and numerical integration techniques. Codes in this portion of the input control output format, convergence criterion on alpha, allowable number of iterations, choice of solution type, and correspondence between the aerodynamic and structural reference points.

Figure 10 shows aerodynamic reference point location, assigned reference areas, planform dimensions and coordinate system. Twenty-eight structural node points, defining a total of twenty-two rectangular and triangular plate elements were selected to analytically describe structural behavior. The material properties and temperatures associated with each node point and structural element are based on experimental data of the previous chapter. For the analyses being considered, the initial loads (both in-plane and out-of-plane), initial displacements and thermal moments are zero. Boundary conditions associated with the analyses are specified by assigning zero linear and angular displacements to the root node points.

Aerodynamic influence coefficient matrices are proportional to those coefficients given in Tables 1 to 3. The initial angle of attack distributions for the planform under study are zero since the specimen remained horizontal during test and in addition had no built-in camber or twist. Integration matrices normally used in static aeroelastic analyses are replaced by special matrices pertinent to this analysis and are given in Table 4. Also included in this table are certain geometric and aerodynamic influence coefficient matrices. As previously mentioned, twenty-eight structural node points were specified. Ten of these correspond to aerodynamic reference points; thus, a distinction between these sets of points must be made. This is accomplished by listing, as program input, those points which are not common to the aerodynamic-aeroelastic analysis.

The analysis method of Reference 1 stipulates that either a closed form or series type solution may be used to obtain the equilibrium angles of attack. In the subject analyses, series type solutions were used and results are designated by types m = 0 and m = 1 respectively. (See Equation (2.20), Reference 1). The closed form solution cannot be used in the present case since the initial angles of attack, $\bar{\alpha}_g$, are zero.

3.3 DISCUSSION OF RESULTS

3.3.1 Influence Coefficient Matrices

Deflection and slope influence coefficients were determined experimentally and serve as comparators to determine the adequacy of the angle measuring

device used in the simulation scheme and to determine the accuracy of the theoretically derived matrices to be used in subsequent theory to test comparisons.

Three sets of experimentally derived influence coefficients were obtained. The first two sets consist respectively of deflection and slope influence coefficients determined from dial gage measurements. Fifteen dial gages were equally spaced about the planform reference points and deflection readings were taken at various load levels. These data were converted to deflection and slope influence coefficients at the planform reference points by applying suitable curve fitting and differentiating techniques. Results are shown in Figures 11 and 12. The third set of experimental coefficients were determined by using the accelerometers mounted at each planform reference point and recording the angular deformation at increasing load levels. Application of a least squares curve fitting technique to the raw data resulted in the slope influence coefficients displayed in Figure 13.

Theoretical deflection and slope influence coefficients were obtained from the plate discrete element relationships developed in connection with the computer program of this study (See Reference 1). Such relationships lead directly to the desired result through matrix inversion techniques. The gridwork of Figure 10 was used to derive the sets of influence coefficients shown in Figures 11 and 13.

Comparison of theoretical and test deflection influence coefficients are shown in Figure 11. Study of these data shows that agreement is within 15% and that the theoretical method of Reference 1 consistently underestimates test values. Although these data are not used in the theory to test comparisons discussed in the next section they do serve as a guideline and indicate that the method of Reference 1 has certain inadequacies. These are discussed further in the next section.

Both sets of experimentally derived slope matrices are compared in Figure 12, Inspection of this figure shows that agreement is within ±10% except for points near the root as would be expected since the angular displacements at these points are relatively small in magnitude. It is pertinent to note that due to the manner in which these data were obtained, a portion of the percentage disagreement can be attributed to data reduction procedures and recording errors. Based on these

comparisons it is concluded that the accelerometer--load cell combination should adequately measure the structural behavior of the test specimen. Thus the "accelerometer" slope influence coefficients shown in Figure 12 serve as a good base for comparisons with theoretically derived slope influence coefficients.

Figure 13 displays a comparison between theoretical and test slope influence coefficients. Study of this figure indicates that an erratic degree of correspondence exists between the sets of data. Certain points are in excellent agreement with test data, while the majority of points are within ±10% of the test values.

The existing disagreement between sets of theoretically derived and experimentally determined deflection and slope influence coefficients may be attributed to several factors. Foremost is the fact that in the present analyses only a limited number of triangular and rectangular plate elements could be used to describe the structural behavior in a region of rapidly changing geometry and spanwise curvature. Increasing the number of structural elements and nodes would demand a revision of the subject computer program and attendant core storage capability. Another possible factor influencing theoretical results is the presence of root flexibility effects. These were seen to be of some consequence in the analyses of the rectangular wing of Reference 1.

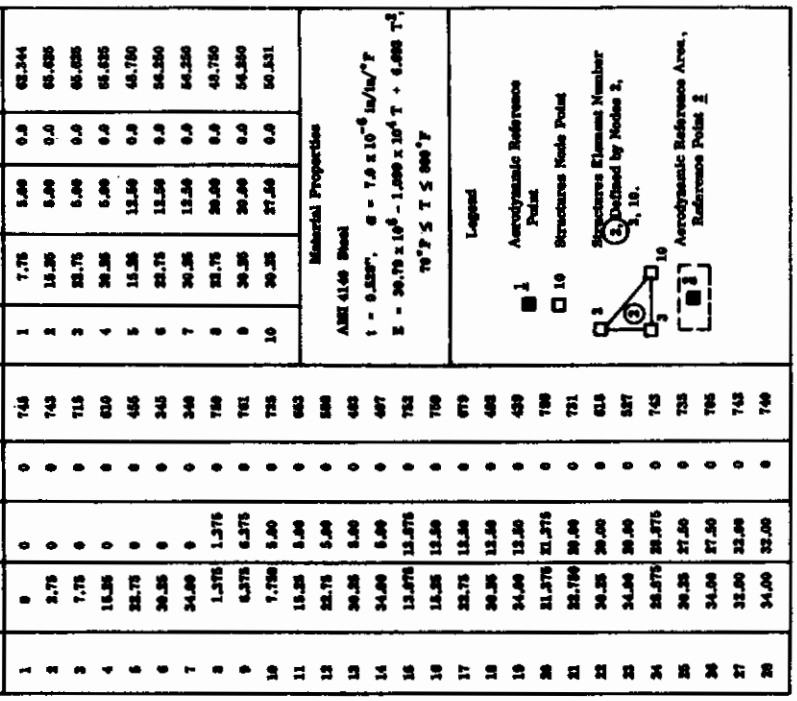

Structure Node Points					Aerodynamic Reference Points				
Point	Coordinates (in.)			Temp. °F	Ref. Point	Coordinates (in.)			Reference Area (in.²)
	X	Y	Z			X	Y	Z	
1	0	0	0	745	1	7.75	5.00	0.0	62.344
2	3.75	0	0	743	2	15.25	5.00	0.0	65.625
3	7.75	0	0	715	3	22.75	5.00	0.0	65.625
4	15.25	0	0	630	4	30.25	5.00	0.0	65.625
5	22.75	0	0	495	5	15.25	12.50	0.0	48.750
6	30.25	0	0	345	6	22.75	12.50	0.0	56.250
7	34.00	0	0	340	7	30.25	12.50	0.0	56.250
8	1.375	1.375	0	720	8	22.75	20.00	0.0	48.750
9	6.375	6.375	0	701	9	30.25	20.00	0.0	54.500
10	7.750	5.00	0	725	10	30.25	27.50	0.0	50.531
11	15.25	5.00	0	662					
12	22.75	5.00	0	588					
13	30.25	5.00	0	483					
14	34.00	5.00	0	497					
15	13.875	13.875	0	752					
16	15.25	12.50	0	709					
17	22.75	12.50	0	670					
18	30.25	12.50	0	486					
19	34.00	12.50	0	450					
20	21.375	21.375	0	720					
21	22.750	20.00	0	721					
22	30.25	20.00	0	615					
23	34.00	20.00	0	557					
24	28.875	28.875	0	745					
25	30.25	27.50	0	733					
26	34.00	27.50	0	705					
27	32.00	32.00	0	745					
28	34.00	32.00	0	740					

Material Properties

AMS 4140 Steel

$\mu = 0.285^{\#}$, $\alpha = 7.0 \times 10^{-6}$ in/in/°F

$E = 30.70 \times 10^{6} - 1.000 \times 10^{4}\,T + 4.000\,T^{2}$,

$70°F \leq T \leq 800°F$

Legend

■ 1 Aerodynamic Reference Point

□ 10 Structures Node Point

Structures Element Number (2) Defined by Nodes 2, 5, 10.

Aerodynamic Reference Area, Reference Point 2

Figure 10. Delta Planform Analysis Input

TABLE 4

AERODYNAMIC, GEOMETRIC AND INTEGRATION MATRICES

Aerodynamic Matrices*					
Ref. Point	$[Q_1]$	$[Q_2]$	$[Q_3]$	$\{\bar{a}\ g\}$	$[R]$
1	-50	500	0	0	62.344
2	-35	500	0	0	65.625
3	-30	350	0	0	65.625
4	+25	200	0	0	65.625
5	-75	200	0	0	48.750
6	-50	350	0	0	56.250
7	-50	350	0	0	56.250
8	-75	200	0	0	48.750
9	-50	350	0	0	56.250
10	-75	350	0	0	50.531
$[Q_a] = [0]$, $Q_b = 0$; q = 6, 8, 10 psi					

$$[I] = [1.0 \quad 1.0 \quad 1.0 \quad 1.0]$$

$$[II] = [0.15625 \quad 0.390625 \quad 0.6250 \quad 0.85938]$$

$$[c/c] = \begin{bmatrix} 1.0 & 0 & 0 & 0 \\ 0 & 1.0 & 0 & 0 \\ 0 & 0 & 1.0 & 0 \\ 0 & 0 & 0 & 1.0 \end{bmatrix}$$

$$[I] = \begin{bmatrix} 0.10823 & 0.11393 & 0.11393 & 0.11393 & 0 & 0 & 0 & 0 & 0 & 0 \\ 0 & 0 & 0 & 0 & 0.10823 & 0.11393 & 0.11393 & 0.11393 & 0 & 0 \\ 0 & 0 & 0 & 0 & 0 & 0 & 0 & 0.08463 & 0.09765 & 0 \\ 0 & 0 & 0 & 0 & 0 & 0 & 0 & 0 & 0 & 0.08772 \end{bmatrix}$$

* Elements of $[Q_o]$ are obtained from elements of $\{P_{z_o}\}$, Tables 1 to 3, using expression $Q_{o_i} = \dfrac{P_{z_{o_i}}}{q\,R_i}$.

$$
\begin{Bmatrix} \delta_{10} \\ \delta_9 \\ \delta_8 \\ \delta_7 \\ \delta_6 \\ \delta_5 \\ \delta_4 \\ \delta_3 \\ \delta_2 \\ \delta_1 \end{Bmatrix} = 10^{-6} \begin{bmatrix}
924.378^{(a)} & 540.060 & 447.797 & 233.240 & 190.099 & 128.608 & 42.553 & 33.708 & 21.546 & 8.686 \\
960.686^{(b)} & 570.748 & 478.144 & 258.943 & 213.361 & 148.222 & 50.419 & 41.190 & 27.431 & 13.259 \\
 & 351.726 & 433.053 & 165.619 & 126.960 & 81.992 & 32.111 & 23.600 & 14.028 & 5.239 \\
573.024 & 378.068 & 280.598 & 184.900 & 144.448 & 98.092 & 41.131 & 29.433 & 18.895 & 7.492 \\
 & & 288.701 & 127.898 & 130.443 & 106.810 & 23.780 & 24.080 & 19.354 & 9.486 \\
479.105 & 305.533 & 354.007 & 144.630 & 143.544 & 113.030 & 28.037 & 29.193 & 23.826 & 12.479 \\
 & & & 95.053 & 65.286 & 37.973 & 21.396 & 13.593 & 6.622 & 2.053 \\
259.347 & 185.684 & 143.423 & 109.517 & 76.471 & 47.740 & 28.281 & 18.281 & 34.762 & 4.290 \\
 & & & & 71.240 & 56.405 & 13.733 & 15.185 & 11.345 & 5.187 \\
214.718 & 145.800 & 144.132 & 78.201 & 79.349 & 66.900 & 18.723 & 19.143 & 8.555 & 8.186 \\
 & & & & & 72.917 & 6.905 & 11.956 & 16.026 & 10.770 \\
155.130 & 100.048 & 124.100 & 48.787 & 68.173 & 81.150 & 10.207 & 16.193 & 24.43 & 14.147 \\
 & & & & & & 8.853 & 3.436 & 1.056 & 2.643 \\
58.339 & 44.710 & 34.083 & 30.062 & 21.035 & 10.854 & 13.207 & 7.896 & 3.378 & 1.349 \\
 & & & & & & & 6.710 & 2.989 & 0.950 \\
48.125 & 34.589 & 34.629 & 13.586 & 20.718 & 17.663 & 7.470 & 8.563 & 6.593 & 3.050 \\
 & & & & & & & & 7.047 & 3.144 \\
30.856 & 20.396 & 26.152 & 12.800 & 16.925 & 20.353 & 3.079 & 5.588 & 7.846 & 5.938 \\
 & & & & & & & & & 7.861 \\
14.624 & 8.545 & 14.274 & 7.809 & 8.513 & 15.148 & 0.688 & 2.398 & 5.383 & 10.020
\end{bmatrix} \begin{Bmatrix} P_{z_{10}} \\ P_{z_9} \\ P_{z_8} \\ P_{z_7} \\ P_{z_6} \\ P_{z_5} \\ P_{z_4} \\ P_{z_3} \\ P_{z_2} \\ P_{z_1} \end{Bmatrix}, \left(\frac{\text{in}}{\text{lb}}\right)
$$

(a) Theoretical Value, Reference 1
(b) Test Value, Dial Gages

Figure 11. Theory-Test Comparisons, Deflection Influence Coefficients Delta Planform

$$
\begin{Bmatrix} \alpha_{10} \\ \alpha_{9} \\ \alpha_{8} \\ \alpha_{7} \\ \alpha_{6} \\ \alpha_{5} \\ \alpha_{4} \\ \alpha_{3} \\ \alpha_{2} \\ \alpha_{1} \end{Bmatrix} = 10^{-6} \begin{bmatrix}
-13.079^{(a)} & -9.925 & 1.1012 & -4.951 & 0.056 & 2.658 & -1.269 & 0.047 & 0.634 & 0.547 \\
-14.594^{(b)} & -10.194 & 1.383 & -5.401 & 0.174 & 2.920 & -1.459 & 0.028 & 0.610 & 0.622 \\
-11.560 & -9.266 & 1.084 & -5.450 & 0.244 & 2.913 & -1.344 & 0.259 & 0.816 & 0.515 \\
-10.411 & -8.889 & 1.437 & -5.300 & 0.448 & 2.991 & -1.423 & 0.362 & 0.656 & 0.596 \\
-13.485 & -10.080 & -1.387 & -5.289 & -0.485 & 3.069 & -1.532 & -0.090 & 0.499 & 0.887 \\
-14.047 & -10.201 & -1.289 & -5.472 & -0.523 & 3.179 & -1.293 & -0.086 & 0.727 & 0.757 \\
-5.456 & -5.180 & 0.7665 & -4.044 & 0.631 & 2.274 & -1.336 & 0.154 & 0.622 & 0.468 \\
-5.197 & -5.067 & 1.2290 & -4.038 & 1.030 & 2.400 & -1.353 & 0.327 & 0.642 & 0.502 \\
-6.696 & -5.582 & -1.206 & -4.118 & -0.207 & 2.531 & -1.209 & -0.032 & 0.631 & 0.614 \\
-7.014 & -5.817 & -1.356 & -4.105 & -0.659 & 2.435 & -1.230 & -0.039 & 0.680 & 0.664 \\
-9.445 & -6.745 & -5.029 & -3.632 & -3.120 & 0.967 & -1.057 & -0.863 & 0.241 & - \\
-8.470 & -6.143 & -4.489 & -3.522 & -2.562 & 1.089 & -0.993 & -0.748 & 0.284 & 1.093 \\
-0.6264 & -0.816 & 0.902 & -1.083 & 0.568 & 0.935 & -0.684 & 0.441 & 0.229 & - \\
-0.8611 & -0.968 & 0.537 & -1.078 & 0.479 & 0.791 & -0.597 & 0.356 & 0.204 & 0.163 \\
-1.928 & -1.661 & -0.557 & -1.293 & -0.238 & 0.737 & -0.752 & -0.045 & 0.410 & - \\
-1.835 & -1.610 & -0.487 & -1.301 & -0.295 & 0.717 & -0.765 & -0.041 & 0.444 & 0.250 \\
-2.543 & -2.039 & -1.635 & -1.349 & -1.221 & -0.105 & -0.446 & -0.487 & 0.004 & 0.360 \\
-1.961 & -1.511 & -1.124 & -0.980 & 0.849 & 0.000 & -0.343 & -0.439 & 0.035 & 0.567 \\
-1.885 & -0.965 & -1.395 & -0.425 & -0.685 & -1.363 & -0.160 & -0.289 & -0.608 & 0.360 \\
-1.963 & -1.382 & -1.651 & -0.670 & -1.047 & -1.208 & -0.230 & -0.293 & -0.513 & 0.467
\end{bmatrix} \begin{Bmatrix} P_{z_{10}} \\ P_{z_{9}} \\ P_{z_{8}} \\ P_{z_{7}} \\ P_{z_{6}} \\ P_{z_{5}} \\ P_{z_{4}} \\ P_{z_{3}} \\ P_{z_{2}} \\ P_{z_{1}} \end{Bmatrix}, \left(\frac{\text{rad}}{\text{lb}}\right)
$$

(a) Dial Gage Test Value

(b) Accelerometer Test Value

Figure 12. Comparison of Dial Gage-Accelerometer Slope Influence Coefficients, Room Temperature, Delta Planform Specimen

$$
\begin{Bmatrix} \alpha_{10} \\ \alpha_9 \\ \alpha_8 \\ \alpha_7 \\ \alpha_6 \\ \alpha_5 \\ \alpha_4 \\ \alpha_3 \\ \alpha_2 \\ \alpha_1 \end{Bmatrix} = 10^{-6} \begin{bmatrix}
-13.752^{(a)} & -9.287 & 2.304 & -5.011 & 0.706 & 3.349 & -1.115 & 0.114 & 0.707 & 0.552 \\
-14.594^{(b)} & -10.194 & 1.383 & -5.401 & 0.174 & 2.920 & -1.459 & 0.028 & 0.610 & 0.622 \\
-9.746 & -8.408 & 2.069 & -4.840 & 0.760 & 3.243 & -1.108 & 0.122 & 0.707 & 0.532 \\
-10.411 & -8.889 & 1.437 & -5.300 & 0.448 & 2.991 & -1.423 & 0.362 & 0.652 & 0.596 \\
-15.031 & -10.495 & -1.043 & -5.309 & 0.163 & 3.419 & -1.122 & 0.013 & 0.698 & 0.615 \\
-14.047 & -10.201 & -1.289 & -5.472 & -0.523 & 3.179 & -1.293 & -0.086 & 0.727 & 0.757 \\
-4.110 & -4.270 & 1.642 & -3.302 & 1.512 & 2.412 & -0.973 & 0.426 & 0.585 & 0.340 \\
-5.197 & -5.067 & 1.229 & -4.038 & 1.030 & 2.400 & -1.353 & 0.327 & 0.642 & 0.502 \\
-6.800 & -5.574 & -0.910 & -3.863 & -0.704 & 2.631 & -0.981 & -0.133 & 0.656 & 0.577 \\
-7.014 & -5.817 & -1.356 & -4.105 & -0.659 & 2.435 & -1.230 & -0.039 & 0.680 & 0.664 \\
-9.240 & -6.351 & -5.328 & -3.486 & -3.086 & 0.674 & -0.812 & -0.755 & 0.584 & 0.942 \\
-8.470 & -6.143 & -4.489 & -3.522 & -2.562 & 1.089 & -0.993 & -0.748 & 0.284 & 1.093 \\
-0.353 & -0.745 & 0.724 & -0.883 & 0.595 & 0.824 & -0.274 & 0.502 & 0.143 & 0.104 \\
-0.8611 & -0.968 & 0.537 & -1.078 & 0.479 & 0.791 & -0.597 & 0.356 & 0.204 & 0.163 \\
-1.703 & -1.355 & -0.531 & -1.105 & -0.166 & 0.608 & -0.678 & -0.052 & 0.573 & 0.087 \\
-1.835 & -1.610 & -0.487 & -1.301 & -0.295 & 0.717 & -0.765 & -0.041 & 0.444 & 0.250 \\
-1.479 & -1.142 & -0.632 & -0.745 & -0.604 & 0.521 & -0.150 & -0.407 & -0.044 & 0.669 \\
-1.961 & -1.511 & -1.124 & -0.980 & -0.849 & 0.0 & -0.343 & -0.439 & 0.035 & 0.567 \\
-1.559 & -0.997 & -1.637 & -0.421 & -0.926 & -1.762 & -0.056 & -0.185 & -0.798 & -0.218 \\
-1.963 & -1.382 & -1.651 & -0.670 & -1.047 & -1.208 & -0.230 & -0.293 & -0.513 & 0.467
\end{bmatrix} \begin{Bmatrix} P_{z_{10}} \\ P_{z_9} \\ P_{z_8} \\ P_{z_7} \\ P_{z_6} \\ P_{z_5} \\ P_{z_4} \\ P_{z_3} \\ P_{z_2} \\ P_{z_1} \end{Bmatrix}, \left(\frac{\text{rad}}{\text{lb}}\right)
$$

(a) Theoretical Value, Reference 1
(b) Test Value, Accelerometers

Figure 13. Theory-Test Comparison, Slope Influence Coefficients
Room Temperature Delta Planform

3.3.2 Aeroelastic Theory to Test Comparisons

Results of room temperature aeroelastic analyses are shown in Table 5 and Figures 14 to 20. Table 6 displays a schedule of these analyses. All analyses shown, except those of Figures 14c and 14d, were accomplished using the digital computer program of Reference 1. Analyses A, B, $\bar{A}$, and $\bar{B}$ represent solutions using the slope influence coefficients shown in Figure 13 and do not include the effects of large deflections. It is assumed that these effects are not significant for the test conditions shown in Figure 14 and thus provide a means for determining the accuracy of the nonlinear aerodynamic-linear structural analysis portion of the computer program. Analyses C to E represent solutions wherein nonlinear aerodynamic and nonlinear structural behavior was considered. Test data are shown by the various symbols.

Figure 14 shows a comparison between test data at the leading edge reference points and Analyses A to $\bar{B}$. Analysis A used accelerometer slope influence coefficients; Analysis B used the theoretical coefficients of Reference 1. It is to be noted here that all other analysis inputs were identical in Analyses A and B.

Examination of the comparisons show that Analysis A results are in close agreement with test points at certain reference stations and, generally, are above test data. Analysis B comparisons range from fair to poor, the latter grade applying particularly to the tip reference points at the q = 10 psi load level. This was to be expected based on the comparisons shown in Figure 13; however, not to the degree shown.

Additional analyses were conducted by calculating equilibrium alphas using test equilibrium loads and the slope influence coefficients of Figure 13. Results are shown in Figures 14c and 14d and are designated as Analyses $\bar{A}$ and $\bar{B}$. (These analyses are counterparts to those shown in Figures 14a and 14b). Examination of these data disclosed that they are generally in closer agreement with the test points. Also, comparison of Figures 14a to 14d reveals differences in theoretical values for each counterpart analysis.

It is apparent from the above results that the disagreement between theory and test values can possibly be attributed to two major factors; namely,

TABLE 5

ROOM TEMPERATURE THEORY TO TEST COMPARISONS,
DELTA WING MODEL

Equilibrium Angle of Attack* (In Degrees)										
Reference Points	q = 6 psi Load Condition 1					q = 8 psi Load Condition 1				
	Test	Analysis				Test	Analysis			
		A	B	$\bar{A}$	$\bar{B}$		A	B	$\bar{A}$	$\bar{B}$
1	-0.0350	-0.0436	-0.0472	-0.0411	-0.0477	-0.0602	-0.0690	-0.0680	-0.0620	-0.0709
2	-0.0202	-0.0262	-0.0082	-0.0243	-0.0098	-0.0375	-0.0430	-0.0125	-0.0373	-0.0159
3	-0.0050	-0.0141	-0.0125	-0.0130	-0.0143	-0.0227	-0.0241	-0.0182	-0.0199	-0.0215
4	+0.0101	+0.0056	+0.0127	+0.0055	+0.0116	+0.0126	+0.0073	+0.0183	+0.0083	+0.0174
5	-0.0979	-0.1068	-0.1129	-0.1000	-0.1210	-0.1550	-0.1741	-0.1646	-0.1518	-0.0183
6	-0.0479	-0.0537	-0.0354	-0.0497	-0.0431	-0.0800	-0.0907	-0.0519	-0.0770	-0.0654
7	-0.0075	-0.0126	+0.0071	-0.0110	+0.0151	-0.0126	-0.0252	+0.0105	-0.0161	+0.0028
8	-0.1029	-0.1123	-0.0965	-0.1051	-0.1111	-0.1606	-0.1850	-0.1391	-0.1573	-0.1645
9	-0.0479	-0.0552	-0.0270	-0.0504	-0.0384	-0.0731	-0.0947	-0.0388	-0.0752	-0.0561
10	-0.0825	-0.0951	-0.0564	-0.0891	-0.0705	-0.1210	-0.1574	-0.0805	-0.1304	-0.1023
Reference Points	q = 10 psi Load Condition 1					q = 10 psi Load Condition 2				
	Test	Analysis				Analysis E				
		A	B	$\bar{A}$	$\bar{B}$	Loop 1	Loop 2	Loop 3	Loop 4	Loop 5
1	-0.1138	-0.1131	-0.0956	-0.1087	-0.1203	-0.1890	-0.2170	-0.2337	-0.2274	-0.2217
2	-0.0685	-0.0724	-0.0179	-0.0677	-0.0232	-0.0490	-0.0859	-0.1151	-0.1237	-0.1220
3	-0.0263	-0.0414	-0.0246	-0.0375	-0.0389	-0.0620	-0.0985	-0.1260	-0.1329	-0.1306
4	+0.0075	+0.0102	+0.0264	+0.0116	+0.0274	+0.0380	+0.0171	0	-0.0092	-0.0097
5	-0.2811	-0.2889	-0.2274	-0.2707	-0.3230	-0.5020	-0.6830	-0.8160	-0.8351	-0.8197
6	-0.1538	-0.1542	-0.0711	-0.1403	-0.1235	-0.2000	-0.3570	-0.4780	-0.5133	-0.5058
7	-0.0351	-0.0476	+0.0177	-0.0382	-0.0039	-0.0240	-0.1400	-0.2300	-0.2630	-0.2595
8	-0.2935	-0.3092	-0.1874	-0.2837	-0.2965	-0.4680	-0.7260	-0.9090	-0.9440	-0.9256
9	-0.1475	-0.1636	-0.0493	-0.1453	-0.1123	-0.1950	-0.4130	-0.5751	-0.6232	-0.6140
10	-0.2359	-0.2646	-0.1059	-0.2400	-0.1909	-0.2960	-0.4970	-0.6261	-0.6404	-0.6232

* Solution type m = 0 shown. Type m = 1 yielded identical results.

TABLE 6

SCHEDULE OF ANALYSES

Analysis	Data Source		
	$\left[\delta_{\alpha z} \right]$	$\left\{ P_z \right\}$	$\left\{ \alpha \right\}$
A	Accelerometers, Figure 13	Program Ref. 1	Program, Ref. 1
B	Program (Ref. 1) Figure 13	Same as A	Same as A
$\overline{A}$	Same as A	Measured Loads, Table 1 - 3	$\left[\delta_{\alpha z}\right] \left\{P_z\right\}$
$\overline{B}$	Same as B	Same as $\overline{A}$	Same as $\overline{A}$
C	Program, Ref. 1	Same as A	Same as A
D	Same as C	Same as A	Same as A
E	Same as C	Same as A	Same as A

TABLE 7

PREDICTION OF "INITIAL ESTIMATE"

$\left\{ \alpha_o \right\}$; q = 10.0, Load Condition No. 1			
	Analysis		
i	A	B	Test
1	-0.0499°	-0.591°	-0.0500°
2	-0.0297	-0.01055	-0.0286
3	-0.0157	-0.01763	-0.0113
4	+0.0073	+0.0148	+0.0075
5	-0.1235	-0.148	-0.1225
6	-0.0609	-0.0516	-0.0650
7	-0.0123	+0.00302	-0.0075
8	-0.1307	-0.1381	-0.1316
9	-0.0619	-0.0450	-0.0588
10	-0.1110	-0.0868	-0.1041

(1) Errors in the numerical iteration technique used in Analyses A and B.

(2) An inadequate structural idealization used to determine slope influence coefficients.

The following paragraphs discuss these two factors.

Additional analyses were performed using test and theoretical slope influence coefficients in a comparable digital computer program which uses the Newton-Raphson technique to solve for the equilibrium alphas. Identical results to those obtained in Analyses A and B were found thereby verifying the existing iteration technique. Further investigation of the numerical iteration technique of Reference 1 showed that the "first-estimate" for alpha is obtained from the following relationship:

$$\{\alpha_o\} = q \left[\delta_{\alpha z}\right]\left[R\right]\left[Q_o\right]\{1\} = \left[\delta_{\alpha z}\right]\{P_{z_o}\} \qquad (5)$$

If this "first-estimate" is in error due to deficiencies in the matrices in Equation (5), particularly $\left[\delta_{\alpha z}\right]$, the solution point or equilibrium angle of attack will be in error since succeeding estimates or iterations will be incorrect as the solution procedure continues. Sets of $\{\alpha_o\}$ were measured during test and comparison of these data with theoretical "first-estimates" are shown in Table 7 for q = 10.0 psi. Analysis A gives closest agreement with test data since all inputs are based on experimental data. Analysis B results are generally below test values. Thus, it would be expected that the numerical iteration technique will not yield correct equilibrium alphas. This is explicitly shown in the sketch of Figure 15a where the "true-case" represents laboratory conditions (see Reference 1 for further discussion). The solution point represents the equilibrium condition attained by satisfaction of the structures and aerodynamic equations. If the slope of the structures equation is in error or deficient in some manner, the solution point will shift from the true case. This effect will be more pronounced as q is increased. Additional investigations into the iteration technique attendant with Analyses A and B produced the results shown in Figure 15b. Examination of these results clearly shows that the iteration technique is highly sensitive to changes in the slope influence coefficient matrix.

Based on the above discussion, several important conclusions can be stated. These are:

1. The nonlinear aerodynamic-linear structures analysis portion of the computer program of Reference 1 can be used with confidence providing the analytical representations of structural behavior and aerodynamic loads are precise.

2. The theoretical slope influence coefficient matrix of Figure 13 is adequate enough in a linear load situation as exemplified in Figure 14d. However, consideration of a nonlinear load situation coupled with an aeroelastic analysis shows that the present formulation of slope influence coefficients can lead to substantial differences between theory and test values. This is explicitly shown in Figure 14b. It is felt that this is due to the triangular-plate elements relationships used and the number of permissible elements in the present computer program.

3. Nonlinear aeroelastic analyses results are very sensitive to changes in the $\left[\delta_{\alpha z} \right]$ matrix. Although the experimental and theoretical slope influence coefficients agreed within ±10% (see Figure 13) use of the latter matrix in the present nonlinear aeroelastic analyses yielded much greater percentage differences.

4. The differences between test and theoretical alphas become more pronounced as q (or the simulated $\bar{\alpha}_g$) is increased due to the presence of the nonlinear aerodynamic terms. This situation becomes critical, of course, as q approaches the divergence dynamic pressure.

It is of interest to note here the work done by Messrs. Durgin and Bartlett (Reference 4). They measured the static aeroelastic deformation and loading of a rectangular wing in supersonic flow where it was assumed that the aerodynamic and structural relationships are linear in nature. Results of their study program showed that the linear aeroelastic solution is sensitive to the aerodynamic matrix $\left[Q \right]$ and the area resolving matrix $\left[R \right]$. This is not the case in the present study since these matrices were determined from test conditions. Attempts by Durgin and Bartlett to predict angular deflections in the same manner as shown in Figures 14c and 14d of this report were not too satisfactory. As discussed in Reference 4,

improvements in theory-test comparisons were effected by deriving elements of the $[R]$ matrix based on bending moments rather than use of Simpson's rule as suggested in Reference 6. The above investigators also suggest that use of more node points to experimentally derive slope influence coefficients would perhaps improve their theory-test comparisons.

Results of attempts to include large deflectional behavior in static aeroelastic analysis will now be discussed. Room temperature test results for q = 10 psi, load condition number three, indicated that the subject test specimen apparently sustained "large deflections" (ratio of tip deflection to plate thickness approximately 5.2), thus this set of test data was chosen for comparative purposes. Analysis results are shown in Figures 16 to 19 in terms of the equilibrium angle of attack at reference point 10, and are denoted as Analysis C and D respectively. Also included are the translational, w_{10}, and angular $\theta_{y_{10}}$, deformations as obtained from the structures portion of the subject computer program.

Figure 16 displays results using the originally coded convergence criteria and iteration technique. In this instance convergence in the structures loop is based on an absolute value test which is applied to each element in the $\{w, \theta_y, \theta_x\}$ matrix. A relative error test is used in the alpha loop. Examination of the results show that a "non-convergent" solution was obtained in the second structures loop; thereby terminating the entire solution procedure. Study of these data and performing additional analyses indicated that the convergence criterion used in the structures loop was perhaps too severe and that more efficient solutions could be obtained if this criterion were relaxed. Actually $\theta_{y_{10}}$ had converged in accordance with the stated criterion.

Based on the above observations a relative error test was coded in the structures subroutine. In addition the iteration technique was changed such that the criterion was applied only to the $\{\theta_y\}$ matrix since this is of direct interest and has the additional effect of improving the efficiency of the computer program. Results of these changes are depicted in Figure 17 as analysis D.

Examination of and comparison of Figure 17 with the preceding figure shows that a "convergent" solution was obtained in the structures loop and a "divergent" solution in the second alpha loop. This would indicate wing divergence. Further examination reveals that the final values of $\theta_{y_{10}}$ and w_{10} are approximately the same as those obtained in Analysis C. The small differences in these values results in changes in the slope influence coefficient matrix which of course affects the static aeroelastic solution. Table 8 shows the main diagonal elements of this matrix for the analyses cited.

TABLE 8

MAIN DIAGONAL ELEMENTS OF SLOPE INFLUENCE COEFFICIENT MATRICES

Ref. Points	Test ($\times 10^{-6}$)	Analysis ($\times 10^{-6}$)			
		B	C	D Loop 1	D Loop 2
1	0.467	-0.218	-0.2159	-0.2158	-0.2137
2	0.035	-0.044	-0.0448	-0.04465	-0.0459
3	-0.041	-0.052	-0.0547	-0.544	-0.0574
4	-0.597	-0.274	-0.2855	-0.2853	-0.2978
5	1.089	0.674	0.747	0.7537	0.8660
6	-0.659	-0.704	-0.8425	-0.8338	-1.001
7	-4.038	-3.302	-3.612	-3.423	-3.585
8	-1.289	-1.043	-1.3971	-1.3538	-1.570
9	-8.889	-8.408	-9.618	-9.571	-11.08
10	-14.594	-13.752	-15.303	-15.17	-16.42

The laboratory tests conducted demonstrated significant static aeroelastic behavior for the largest initial test conditions but of course did not demonstrate wing divergence. Figure 18 displays an analytical representation of the equilibrium angle of attack at reference point ten versus the ratio of the nonlinear divergence dynamic pressure to the linear divergence dynamic pressure. This figure was prepared with the use of the test coefficients in Figure 13 and Table 4. Examination of Figure 18

shows that wing divergence is an explosive type of instability for the present test specimen and nonlinear aerodynamic relationships used. Analyses C and D conditions lie in a critical region and as discussed in Reference 7 divergence will rapidly occur for slight increases in $\{\bar{\alpha}_g\}$. It is felt that the results of Analysis D are caused by the relative changes between test and theoretical slope influence coefficients and the closeness of test conditions to the analytical divergence conditions.

Additional study of Figures 16, 17, and Table 8 reveals that the stiffening effect of large deflectional theory is present. The w loops of Figures 16 and 17 show that the deflections have decreased from their initial values indicating that the plate is stiffening (through decreasing magnitudes of elements in the w - P_z portion of the master stiffness matrix). Inspection of the θ_y loops however shows that the angular deflections have increased which would appear to be a contradiction. The increase or decrease in θ_y due to large deflectional behavior apparently is a function of the relative decrease in the translational deflection w and wing geometry. In the present case these factors have combined to produce increases in θ_y as shown in Figure 19. In this figure the initial and final deflections at node points 21, 22, and 23 (see Figure 10) are displayed for each iterative loop. The local slopes at these nodes are shown in parentheses. The inclusion of large deflection effects is clearly shown on this figure. Nonlinear structural analyses of the rectangular wing model of Reference 1 displayed the opposite results; that is a decrease in translational deflections produced decreasing angular deflections.

In summary, Analyses C and D show that the resulting slope influence coefficient matrix is sensitive to the convergence criterion used and that the equilibrium alpha solution again demonstrates reliance upon accurate slope influence coefficient matrices. It must be remarked that none of the above difficulties were experienced in the analysis of the rectangular wing model as reported in Reference 1, except perhaps for the elevated temperature cases. It can only be concluded that the main difference lies in the inclusion of and the relationships used for the triangular plate elements. The proof of this is beyond the scope of the present study. Additionally, the inclusion of large deflection effects will prove to be significant and can affect static aeroelastic solutions to a great degree as shown below.

The final set of theory - test comparisons obtained, Analysis E, are displayed in Figure 20. The open symbols represent initial "rigid" wing values; the closed symbols represent final "flexible" wing values. Convergence in the major alpha loops was not obtained due to a one hour time limit imposed on machine computations. Examination of the fourth and fifth loops however show that the convergence condition was being approached. The present analysis overestimates the outboard test points by a significant amount, however each set of alpha values progress away from the rigid wing condition towards the flexible wing condition as expected.

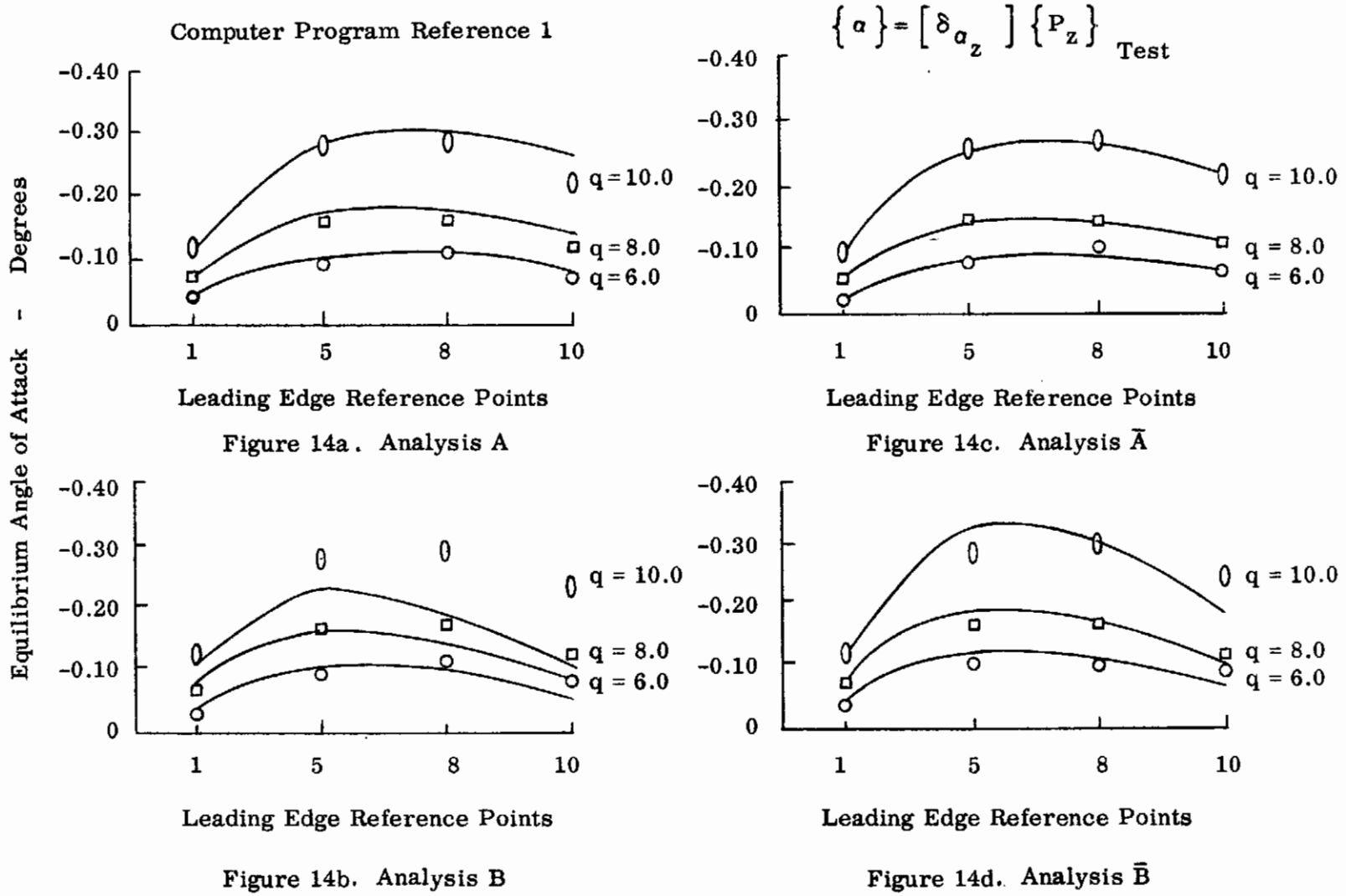

Figure 14a. Analysis A

Figure 14c. Analysis $\bar{A}$

Figure 14b. Analysis B

Figure 14d. Analysis $\bar{B}$

Figure 14. Linear Theory-Test Comparisons, Room Temperature Load Condition No. 1

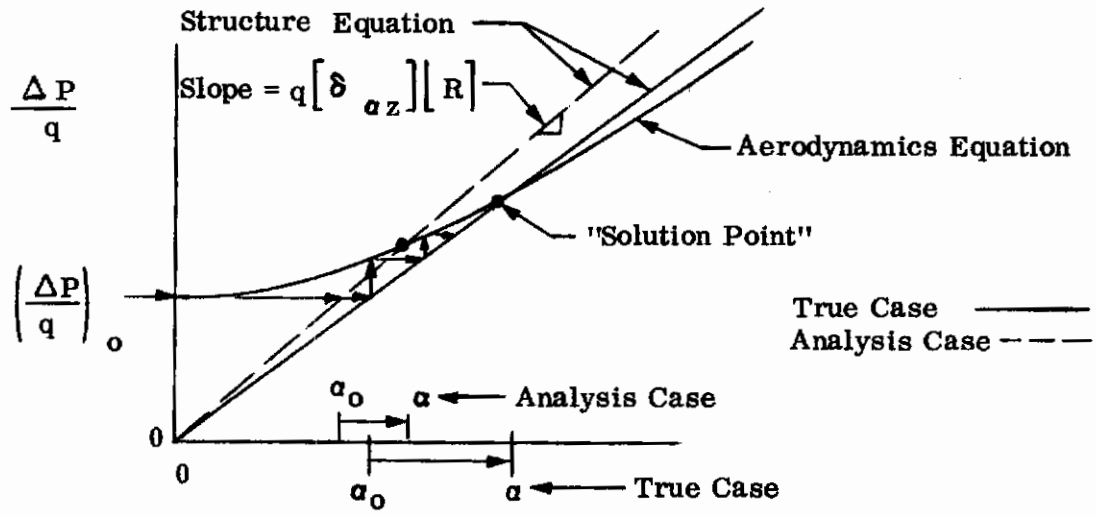

Figure 15a. Illustration of Iteration Technique

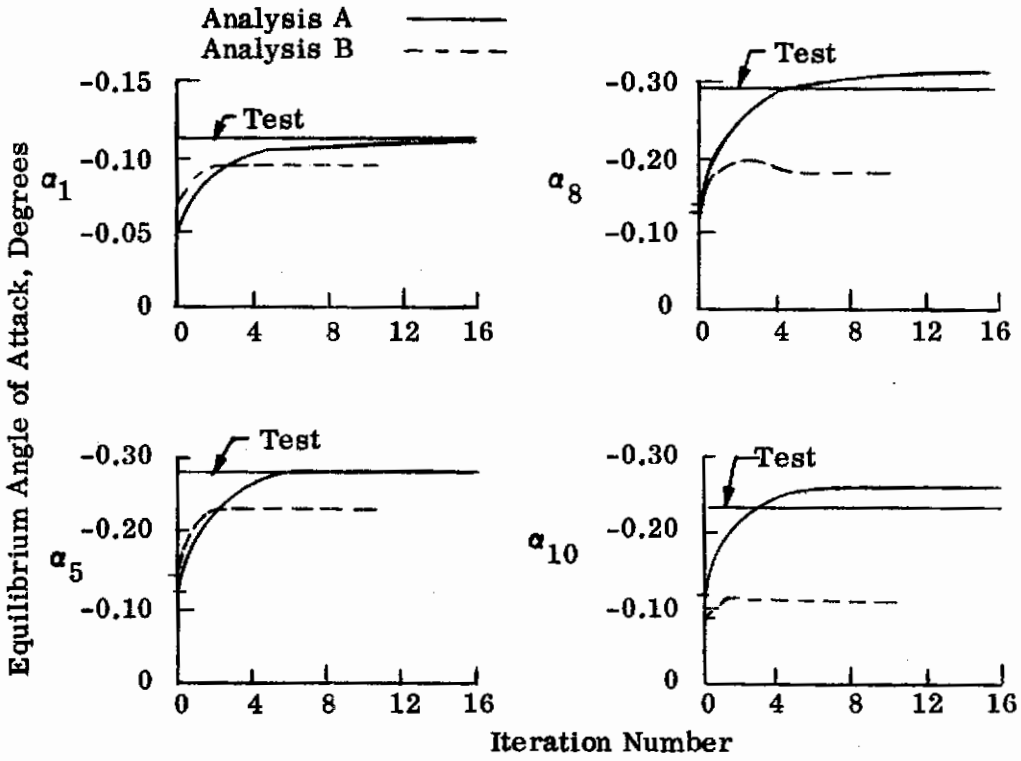

Figure 15b. Typical Iterative Solutions

Figure 15. Numerical Iteration Technique

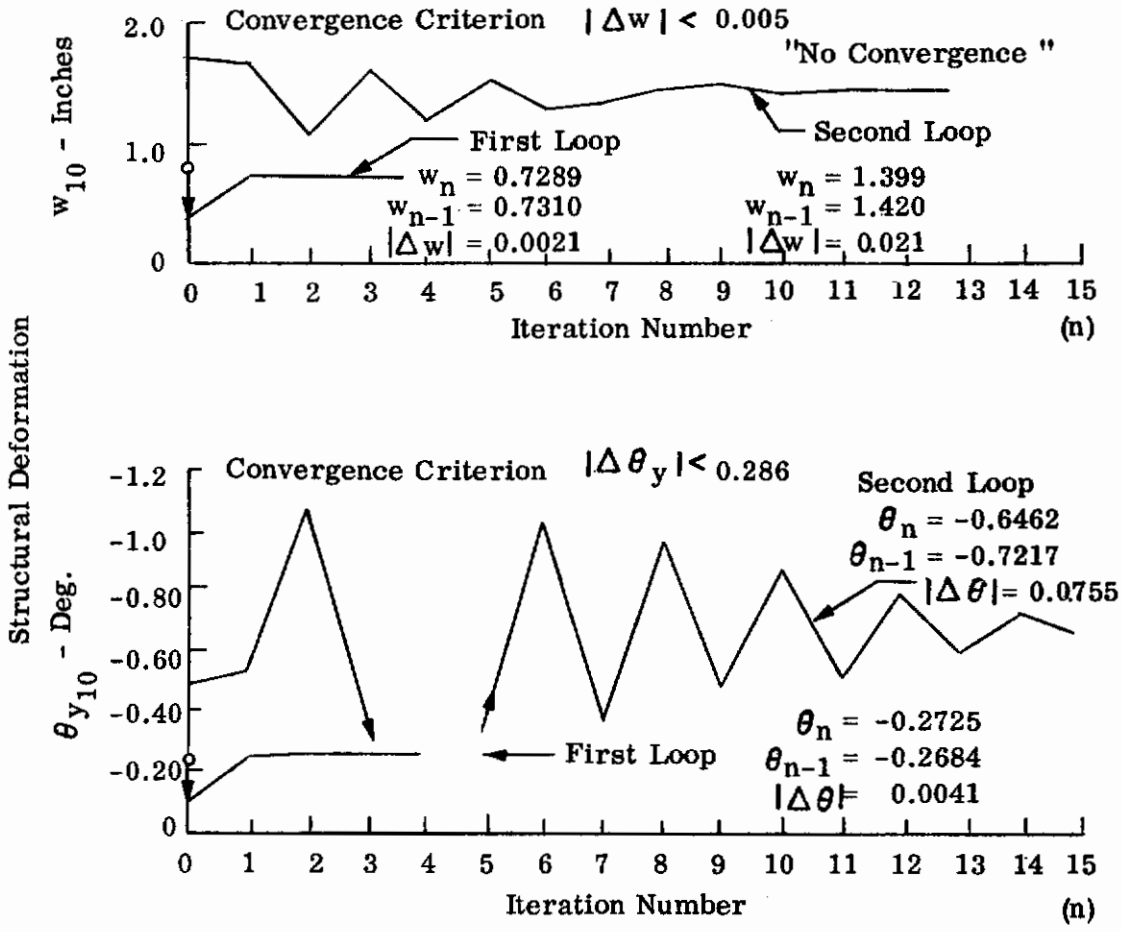

Figure 16a. Structures Loop

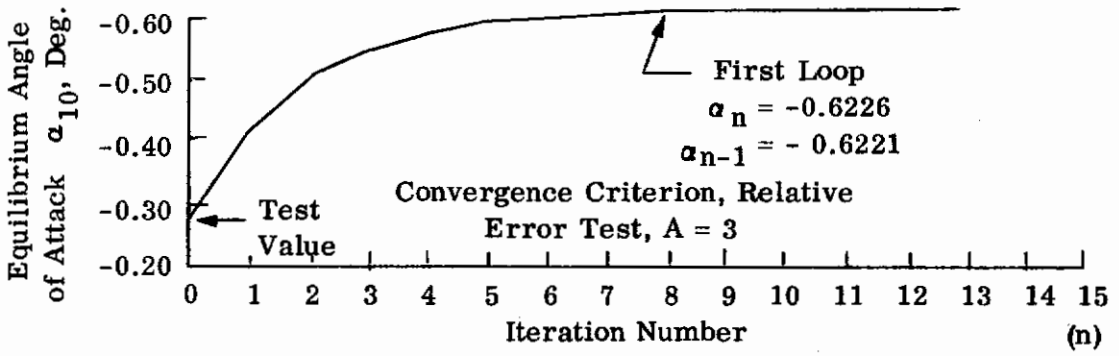

Figure 16b. Alpha Loop

Figure 16. Iteration Paths, Analysis C Room Temperature, q = 10, Load Condition No. 3

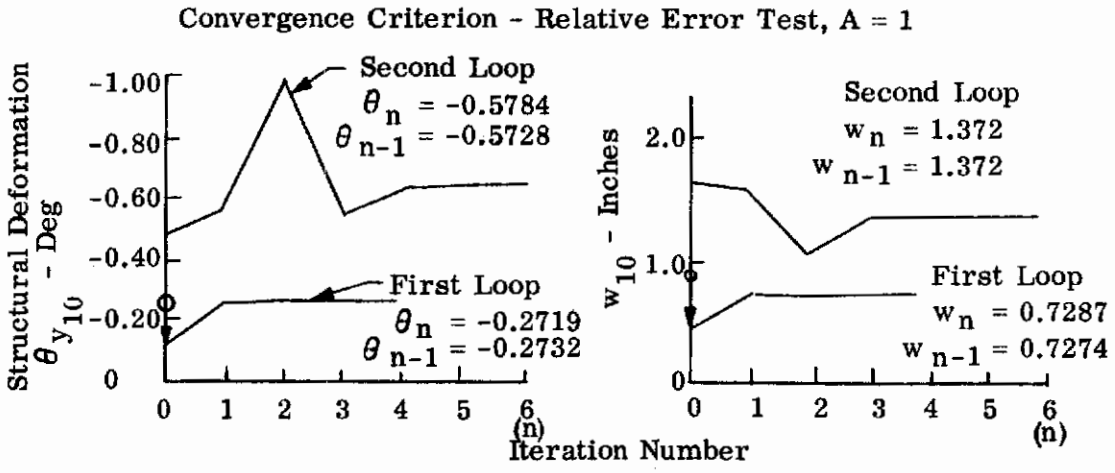

Figure 17a. Structures Loops

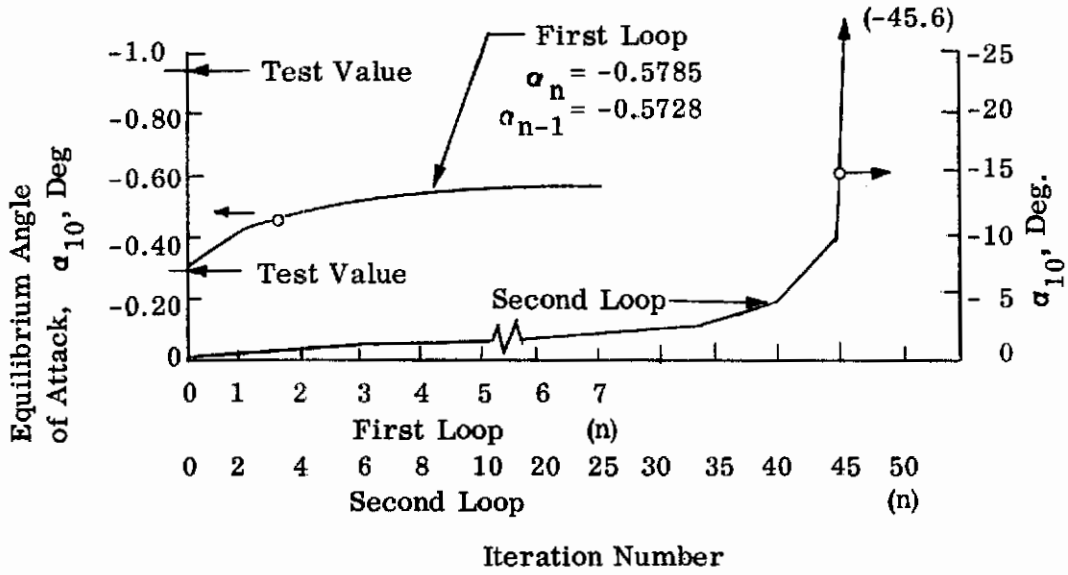

Figure 17b. Alpha Loops

Figure 17. Iteration Paths, Analysis D. Room Temperature q = 10, Load Condition No. 3

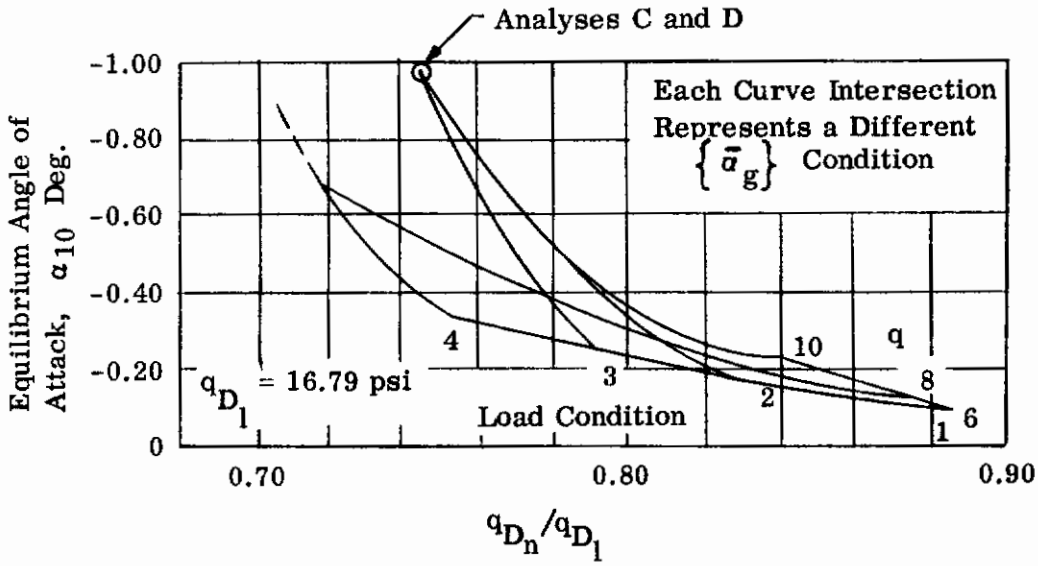

Figure 18. Divergence Dynamic Pressure

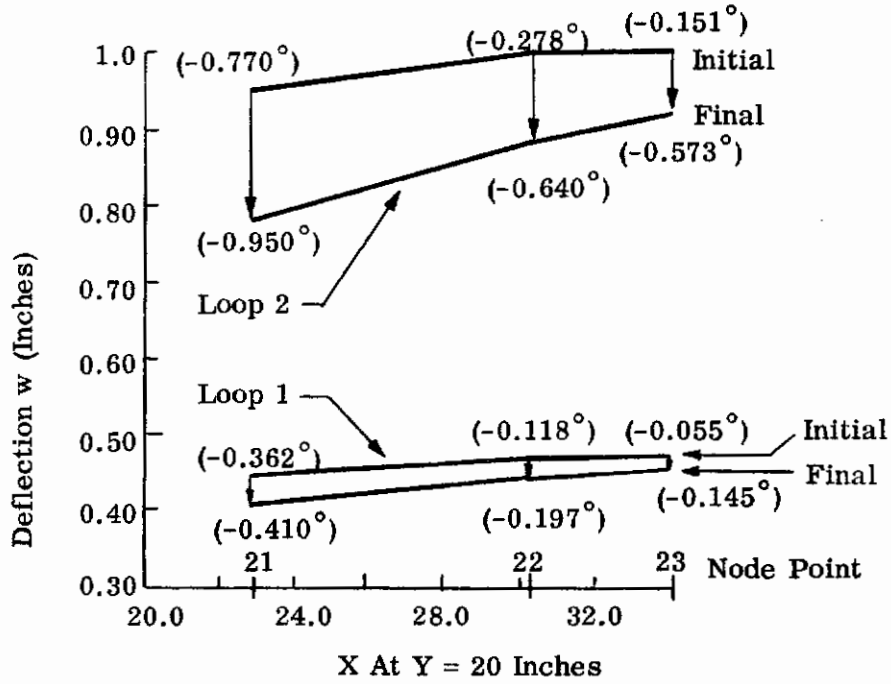

Figure 19. Initial and Final Deflections, Analysis D

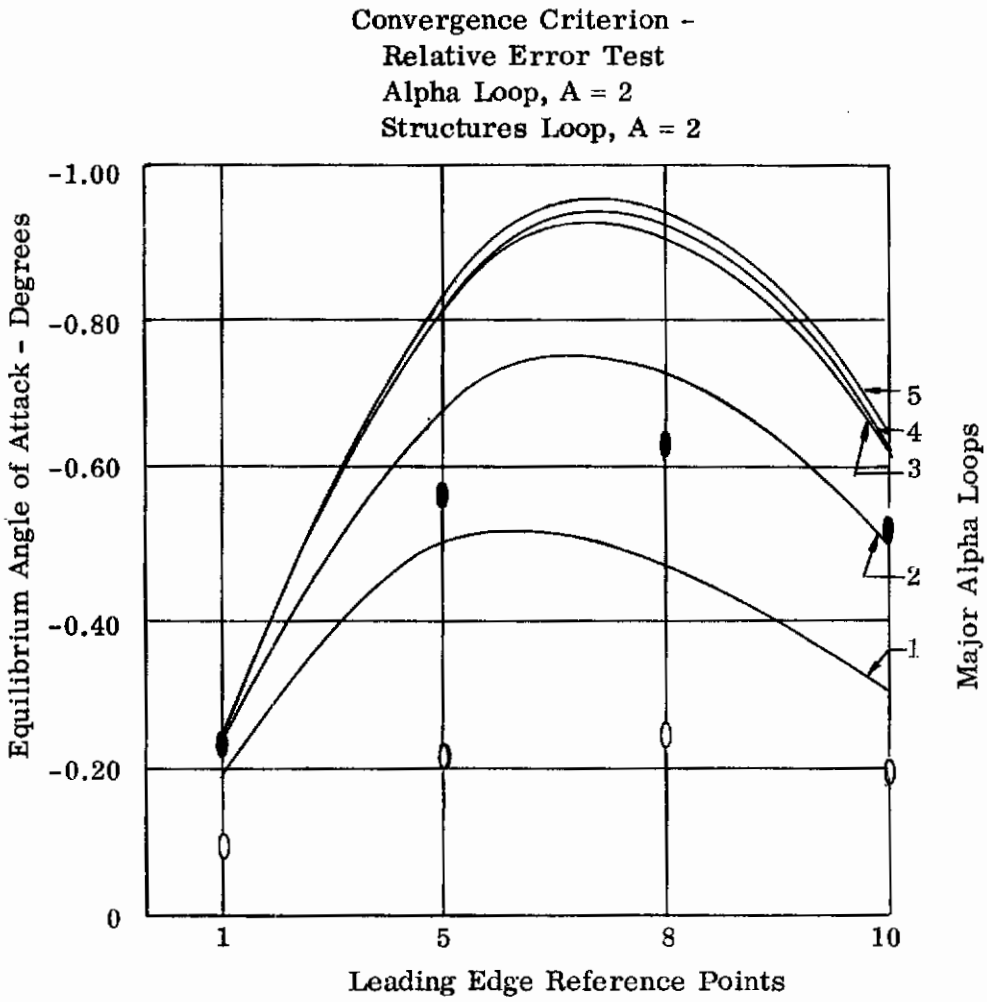

Figure 20. Nonlinear Theory - Test Comparisons - Room Temperature, q = 10 psi, Load Condition No. 2. Analysis E

SECTION 4.0

SUMMARY AND RECOMMENDATIONS

This report has described the simulation and measurement of static aeroelastic behavior in the presence of aerodynamic and structural nonlinearities and elevated temperatures. The simulation scheme described was successfully employed in the measurement of aeroelastic data under the cited conditions. It was concluded from analyses of test data that the interplay between aerodynamic and structural nonlinearities (through geometric large deflections and thermal effects) is significant and of importance in determining static aeroelastic behavior and attendant "flexible" stability and control derivatives. Additionally the test data collected provided an excellent basis for evaluation of theoretical methods.

Comparison of theoretical results, based on the digital computer program of Reference 1, with selected test data showed that:

(1) The computer program is operationally correct.

(2) The nonlinear aerodynamic - linear structures portion of the program can be used with confidence providing that the representation of structural behavior and aerodynamic loads is precise.

(3) The nonlinear aeroelastic analysis solution procedure is very sensitive to small changes in the slope influence coefficient matrix and convergence criterion. This is especially evident for the delta wing model.

(4) The theoretical slope influence coefficient method coded in the computer program is satisfactory for linear load situations. Consideration of nonlinear load situations coupled with nonlinear aeroelastic analysis indicates that the present formulation of slope influence coefficients can lead to substantial differences between theory and test values.

(5) Inclusion of severe deflectional behavior in nonlinear static aeroelastic analysis has resulted in erroneous predictions or no prediction at all. Thus an inadequacy is present in the formulation of the nonlinear terms in the structural analysis portion of the computer program.

(6) Consideration of "large deflection effects" may result in an increase in local streamwise angular deflections although the above effects theoretically stiffen the structure. This phenomenon apparently is a function of the relative decrease in the translational deflections, aerodynamic load distribution and wing planform geometry.

The results of this portion of the study program and those cited in Reference 1 define the present usefulness of the digital computer program. In its present form it

is capable of furnishing acceptable results for linear structural behavior. Its use in nonlinear structural-aeroelastic analysis, in cases of severe deflectional behavior, apparently will not be satisfactory. Based on these conclusions it is recommended that:

(1) The nonlinear structure-nonlinear aerodynamic interaction computer program should be improved so that it can be used with confidence.

(2) The accuracy and convergence characteristics of the digital computer program should be improved by the development of more satisfactory nonlinear terms in the discrete element force-displacement equations. (Present developments are detailed in Reference 1).

(3) The efficiency (i.e., speed) of the developed computer program should be improved through a study of the iterative solution processes, the convergence criteria and the improvement thereof.

(4) Additional theory-test comparisons, utilizing information and developments from Items (1) to (3), should be accomplished in order to check the "improvements" made in these and other computer programs.

This report concludes a series of efforts on hypersonic aerodynamic-structural interactions as they affect static stability and control. The overriding theme for the series (partly reported in References 1 and 8) has been the definition of an appropriate analytical model simulating the interaction. Thus far attempts have not been rewarded with complete success but a solid foundation of useful data and techniques has been gained and the nature of future difficulties in obtaining adequate structural element relationships and convergent solutions has been pointed out. The immediate steps for future work have been listed above. In addition to these, some of the more obvious problems needing attention are:

(1) Development of methods for testing vehicles in the hypersonic regime for specification compliance and verification of engineering design criteria.

(2) Development of methods for including the effects of cumulative structural change and damage in the estimates for flexible vehicle characteristics.

(3) Extension of current methods to include the effects of advanced structural concepts (e.g., cryogenic structures, non-plate-like wing body combinations).

(4) Improvement in current aerodynamic analysis techniques to include interference effects, the interaction of various points in the flow field, the effects of mass addition to the boundary layer and many other aspects in the hypersonic aerodynamic spectrum.

SECTION 5.0

REFERENCES

1. Batt, J.R. and Gallagher, R.H., "Nonlinear Thermoelastic Effects on Hypersonic Stability and Control", Part II Analytical and Experimental Static Aerothermoelasticity, FDL-TDR-64-16, October 1964.

2. Batt, J.R., "Nonlinear Thermoelastic Effects on Hypersonic Stability and Control" Part I, Vols. 1 and 2 Aerodynamics FDL-TDR-64-16 September 1964.

3. Padlog, J. and Gallagher, R.H. "Measurement of Angular Displacements of Practical Wing Structures by the Moire'-Fringe Technique", FDL-TDR-64-42, September 1964.

4. Durgin, F.H. and Bartlett, C.J., "A Measurement of the Static Aeroelastic Deformation and Loading of a Wing in Supersonic Flow", ASD-TDR-63-366, September 1963.

5. Bennett, F.V. "Comparison of Experimental and Theoretical Static Aeroelastic Loads and Deflections of a Thin 45° Delta Wing in Supersonic Flow", NACA TND-974, October 1961.

6. Donato, V.W. "Supersonic Aeroelastic Effects on Static Stability and Control", Part III, Aeroelastic Interaction, WADC TR58-95, July 1960.

7. Padlog, J., Donato, V.W., and Batt, J.R. "Thermoelastic Effects on Hypersonic Stability and Control", Part III Hypersonic Aeroelasticity, ASD-TR-61-287, May 1963.

8. Gallagher, R.H., and Huff, R.D., "Thermoelastic Effects on Hypersonic Stability and Control", Part II, Vol. I Elastic Response Determinations for Severely Heated Wings, ASD-TR-61-287, Part II, Vol. I, August 1962.

UNCLASSIFIED
Security Classification

DOCUMENT CONTROL DATA - R&D
(Security classification of title, body of abstract and indexing annotation must be entered when the overall report is classified)

1. ORIGINATING ACTIVITY (Corporate author)
Bell Aerospace Corporation
Buffalo, N. Y.

2a. REPORT SECURITY CLASSIFICATION
UNCLASSIFIED

2b. GROUP
N/A

3. REPORT TITLE
Nonlinear Thermoelastic Effects on Hypersonic Stability and Control
Part III Simulation, Measurement and Analysis of Nonlinear Static Aerothermoelastic Behavior of a 45° Delta Wing

4. DESCRIPTIVE NOTES (Type of report and inclusive dates)
Final Report

5. AUTHOR(S) (Last name, first name, initial)
Batt, James R.

6. REPORT DATE	7a. TOTAL NO. OF PAGES	7b. NO. OF REFS
December 1964	Approx 49	5

8a. CONTRACT OR GRANT NO.	9a. ORIGINATOR'S REPORT NUMBER(S)
AF33(657)-7486	FDL-TDR-64-16 Pt III
b. PROJECT NO. 8219	
c.	9b. OTHER REPORT NO(S) (Any other numbers that may be assigned this report) None
d.	

10. AVAILABILITY/LIMITATION NOTICES
No limitations

11. SUPPLEMENTARY NOTES	12. SPONSORING MILITARY ACTIVITY
None	Air Force Flight Dynamics Lab (FDCC) Wright-Patterson AFB, Ohio 45433

13. ABSTRACT

Results are presented of additional nonlinear structural-aerodynamic interaction experiments and analyses conducted on a 45° delta wing. The aeroelastic simulation scheme developed and described in FDL TDR 64-16, Part II was used to experimentally determine the static aerothermoelastic behavior of the subject model wing. Test data have been compared with theoretical predictions using the digital computer program developed and described in FDL TDR 64-16, Part II.

DD FORM 1 JAN 64 1473

UNCLASSIFIED
Security Classification

14. KEY WORDS	LINK A		LINK B		LINK C	
	ROLE	WT	ROLE	WT	ROLE	WT
Structural deflection, heated aeroelastic loads, nonlinear aerothermoelastic interaction tests						

INSTRUCTIONS

1. ORIGINATING ACTIVITY: Enter the name and address of the contractor, subcontractor, grantee, Department of Defense activity or other organization *(corporate author)* issuing the report.

2a. REPORT SECURITY CLASSIFICATION: Enter the overall security classification of the report. Indicate whether "Restricted Data" is included. Marking is to be in accordance with appropriate security regulations.

2b. GROUP: Automatic downgrading is specified in DoD Directive 5200.10 and Armed Forces Industrial Manual. Enter the group number. Also, when applicable, show that optional markings have been used for Group 3 and Group 4 as authorized.

3. REPORT TITLE: Enter the complete report title in all capital letters. Titles in all cases should be unclassified. If a meaningful title cannot be selected without classification, show title classification in all capitals in parenthesis immediately following the title.

4. DESCRIPTIVE NOTES: If appropriate, enter the type of report, e.g., interim, progress, summary, annual, or final. Give the inclusive dates when a specific reporting period is covered.

5. AUTHOR(S): Enter the name(s) of author(s) as shown on or in the report. Enter last name, first name, middle initial. If military, show rank and branch of service. The name of the principal author is an absolute minimum requirement.

6. REPORT DATE: Enter the date of the report as day, month, year; or month, year. If more than one date appears on the report, use date of publication.

7a. TOTAL NUMBER OF PAGES: The total page count should follow normal pagination procedures, i.e., enter the number of pages containing information.

7b. NUMBER OF REFERENCES: Enter the total number of references cited in the report.

8a. CONTRACT OR GRANT NUMBER: If appropriate, enter the applicable number of the contract or grant under which the report was written.

8b, 8c, & 8d. PROJECT NUMBER: Enter the appropriate military department identification, such as project number, subproject number, system numbers, task number, etc.

9a. ORIGINATOR'S REPORT NUMBER(S): Enter the official report number by which the document will be identified and controlled by the originating activity. This number must be unique to this report.

9b. OTHER REPORT NUMBER(S): If the report has been assigned any other report numbers *(either by the originator or by the sponsor)*, also enter this number(s).

10. AVAILABILITY/LIMITATION NOTICES: Enter any limitations on further dissemination of the report, other than those imposed by security classification, using standard statements such as:

(1) "Qualified requesters may obtain copies of this report from DDC."

(2) "Foreign announcement and dissemination of this report by DDC is not authorized."

(3) "U. S. Government agencies may obtain copies of this report directly from DDC. Other qualified DDC users shall request through _____."

(4) "U. S. military agencies may obtain copies of this report directly from DDC. Other qualified users shall request through _____."

(5) "All distribution of this report is controlled. Qualified DDC users shall request through _____."

If the report has been furnished to the Office of Technical Services, Department of Commerce, for sale to the public, indicate this fact and enter the price, if known.

11. SUPPLEMENTARY NOTES: Use for additional explanatory notes.

12. SPONSORING MILITARY ACTIVITY: Enter the name of the departmental project office or laboratory sponsoring *(paying for)* the research and development. Include address.

13. ABSTRACT: Enter an abstract giving a brief and factual summary of the document indicative of the report, even though it may also appear elsewhere in the body of the technical report. If additional space is required, a continuation sheet shall be attached.

It is highly desirable that the abstract of classified reports be unclassified. Each paragraph of the abstract shall end with an indication of the military security classification of the information in the paragraph, represented as *(TS), (S), (C), or (U)*.

There is no limitation on the length of the abstract. However, the suggested length is from 150 to 225 words.

14. KEY WORDS: Key words are technically meaningful terms or short phrases that characterize a report and may be used as index entries for cataloging the report. Key words must be selected so that no security classification is required. Identifiers, such as equipment model designation, trade name, military project code name, geographic location, may be used as key words but will be followed by an indication of technical context. The assignment of links, rules, and weights is optional.